NASA/TM—2017-219444

Unusual Oxidative Limitations for Al-MAX Phases

James L. Smialek
Glenn Research Center, Cleveland, Ohio

February 2017

NASA STI Program . . . in Profile

Since its founding, NASA has been dedicated to the advancement of aeronautics and space science. The NASA Scientific and Technical Information (STI) Program plays a key part in helping NASA maintain this important role.

The NASA STI Program operates under the auspices of the Agency Chief Information Officer. It collects, organizes, provides for archiving, and disseminates NASA's STI. The NASA STI Program provides access to the NASA Technical Report Server—Registered (NTRS Reg) and NASA Technical Report Server—Public (NTRS) thus providing one of the largest collections of aeronautical and space science STI in the world. Results are published in both non-NASA channels and by NASA in the NASA STI Report Series, which includes the following report types:

- TECHNICAL PUBLICATION. Reports of completed research or a major significant phase of research that present the results of NASA programs and include extensive data or theoretical analysis. Includes compilations of significant scientific and technical data and information deemed to be of continuing reference value. NASA counter-part of peer-reviewed formal professional papers, but has less stringent limitations on manuscript length and extent of graphic presentations.

- TECHNICAL MEMORANDUM. Scientific and technical findings that are preliminary or of specialized interest, e.g., "quick-release" reports, working papers, and bibliographies that contain minimal annotation. Does not contain extensive analysis.

- CONTRACTOR REPORT. Scientific and technical findings by NASA-sponsored contractors and grantees.

- CONFERENCE PUBLICATION. Collected papers from scientific and technical conferences, symposia, seminars, or other meetings sponsored or co-sponsored by NASA.

- SPECIAL PUBLICATION. Scientific, technical, or historical information from NASA programs, projects, and missions, often concerned with subjects having substantial public interest.

- TECHNICAL TRANSLATION. English-language translations of foreign scientific and technical material pertinent to NASA's mission.

For more information about the NASA STI program, see the following:

- Access the NASA STI program home page at http://www.sti.nasa.gov

- E-mail your question to help@sti.nasa.gov

- Fax your question to the NASA STI Information Desk at 757-864-6500

- Telephone the NASA STI Information Desk at 757-864-9658

- Write to:
  NASA STI Program
  Mail Stop 148
  NASA Langley Research Center
  Hampton, VA 23681-2199

NASA/TM—2017-219444

Unusual Oxidative Limitations for Al-MAX Phases

James L. Smialek
Glenn Research Center, Cleveland, Ohio

National Aeronautics and
Space Administration

Glenn Research Center
Cleveland, Ohio 44135

February 2017

This report contains preliminary findings, subject to revision as analysis proceeds.

Level of Review: This material has been technically reviewed by technical management.

Available from

NASA STI Program
Mail Stop 148
NASA Langley Research Center
Hampton, VA 23681-2199

National Technical Information Service
5285 Port Royal Road
Springfield, VA 22161
703-605-6000

This report is available in electronic form at http://www.sti.nasa.gov/ and http://ntrs.nasa.gov/

Unusual Oxidative Limitations for Al-MAX Phases

James L. Smialek
National Aeronautics and Space Administration
Glenn Research Center
Cleveland, Ohio 44135

Abstract

Alumina-forming MAX phases are well-known for their excellent oxidation resistance, rivaling many metallic NiAl, NiCrAl, and FeCrAl counterparts and with upper temperature capability possible to ~1400 °C. However a number of limitations have been emerging that need to be acknowledged to permit robust performance in demanding applications. Ti_2AlC and Ti_3AlC_2 possess excellent scale adhesion, cyclic oxidation/moisture/volatility resistance, and TBC compatibility. However they are very sensitive to Al content and flux in order to maintain an exclusive Al_2O_3 scale without runaway oxidation of ubiquitous TiO_2 transient scales. Accelerated oxidation has been shown to occur for Al-depleted, damaged, or roughened surfaces at temperatures less than 1200 °C.

Conversely, Cr_2AlC is less sensitive to transients, but exhibits volatile losses at 1200 °C or above if common Cr_7C_3 impurity phases are present. Poor scale adhesion is exhibited after oxidation at 1150 °C or above, where spallation occurs at the Cr_7C_3 (depletion zone) interface. Delayed spallation is significant and suggests a moisture-induced phenomenon similar to non-adherent metallic systems. Re-oxidation of this surface does not reproduce the initial pure Al_2O_3 behavior, but initiates a less-protective scale. Cr_2AlC has also been shown to have good long term bonding with superalloys at 800 °C, but exhibits significant β-NiAl + Cr_7C_3 diffusion zones at 1100 °C and above. This may set limits on Cr_2AlC as a high temperature TBC bond coat on Ni-based superalloys, while improving corrosion resistance in lower temperature applications.

Introduction

MAX phase materials are unique ceramic structures with superb thermal fatigue resistance, good high temperature stability, machinability, damage tolerance, and many other attractive properties (Ref. 1). Among the 60 or so reported compositions, those with Al demonstrate the best high temperature oxidation resistance, primarily Ti_3AlC_2, Ti_2AlC, and Cr_2AlC (Ref. 2). Oxidation kinetics have been studied intensively, and the excellent oxidation resistance is generally attributed to the slow growing protective Al_2O_3 scale. Rate control by Al_2O_3 scale formation on Al-MAX phases is analogous to that measured on oxidation resistant Al_2O_3 forming metallic alloys and subject to a similar time/temperature response envelope. Furthermore, scale adhesion is excellent on $Ti_{2x}AlC_{(2x-1)}$ MAX phases due in part to the excellent and preferred CTE match with Al_2O_3 scales. Thermal shock is generally a non-issue because of the unique structure of the MAX phases, their high thermal conductivity, and acceptable fracture strengths and toughness.

These features indicate that high performing oxidation resistant MAX phase materials may be suitable in elevated temperature, thermally stressed environments. However, there are a number of emerging, somewhat subtle oxidative shortcomings that may hamper utilization of the materials at their full potential. Ti-Al-C MAX phases suffer from preferential TiO_2 formation and growth under special conditions. The Cr_2AlC MAX phase may exhibit massive Al_2O_3 scale spallation to a less protective, but prevalent, Cr_7C_3 depletion zone phase. It is therefore the purpose of this monograph to summarize some current, though incomplete, issues, as a forewarning lest these weaknesses be overlooked. Some areas for property improvements are accordingly suggested as well. This research is on-going on many fronts and needs additional study to be fully complete. Thus various items are included as unpublished data.

Breakaway Oxidation of TiO_2

Reduction in the Al Content of Ti_3AlC_2

The oxidation of Ti_3AlC_2, Ti_2AlC, and Cr_2AlC has been critically reviewed (Ref. 2). The steady state kinetics have been analyzed as cubic, not parabolic. This is because grain growth in the scale causes the continuous reduction of grain boundaries which serve as short-circuit, rate-controlling diffusion paths in Al_2O_3. Furthermore, the outer scale surface is universally found to contain TiO_2-rich nodules which generally do not seem to increase, but rather remain as a vestige of early, low temperature transient growth (Refs. 3 to 8). One study did however find low temperature breakaway oxidation due to promulgated formation of non-protective TiO_2 at 600 °C. Others show that the TiO_2 transient is limited to the first few minutes of oxidation during heating to higher temperatures, then stabilizes with time as distinctive granular clusters (Refs. 7, 9, and 10) (Fig. 1, Figs. 2(a) and (b)). Subsequent cubic kinetics were seen to be consistent with grain boundary diffusivity of oxygen (Refs. 7, 11, and 12).

The alumina scale growth rates can be used to project best case scenarios from a mass balance. (Al supply reservoir) argument. That is, the compound would not be expected to continue to form a protective alumina scale after all the aluminum in the object were consumed. But, more restrictively, it has been proposed that a "critical" Al level is required at the scale-MAX phase interface to allow an existing Al_2O_3 scale to continue to form exclusively (Ref. 13). Here TiO_2 breakaway was observed to form on Ti_3AlC_2 after 3000 h at 1100 °C, corresponding to an Al/Ti ratio of ~0.91/3 (Figs. 3(a) (b)). This event was manifested as a jump from a protective 12 μm Al_2O_3 scale at 3250 h, with some large formed TiO_2 nodules, culminating in complete consumption of the 2 mm thick sample at 4000 h. In brief, the loss of Al is associated with an inability to maintain Al_2O_3 control, allowing TiO_2 to progressively increase, leading to eventual breakaway because of rapid diffusion in TiO_2. (However, in an unrelated study, it was shown that Ti_2AlC survived 500 h oxidation at 1300 °C and Al_2O_3 scales on the order of 35 to 40 μm) (Ref. 14).

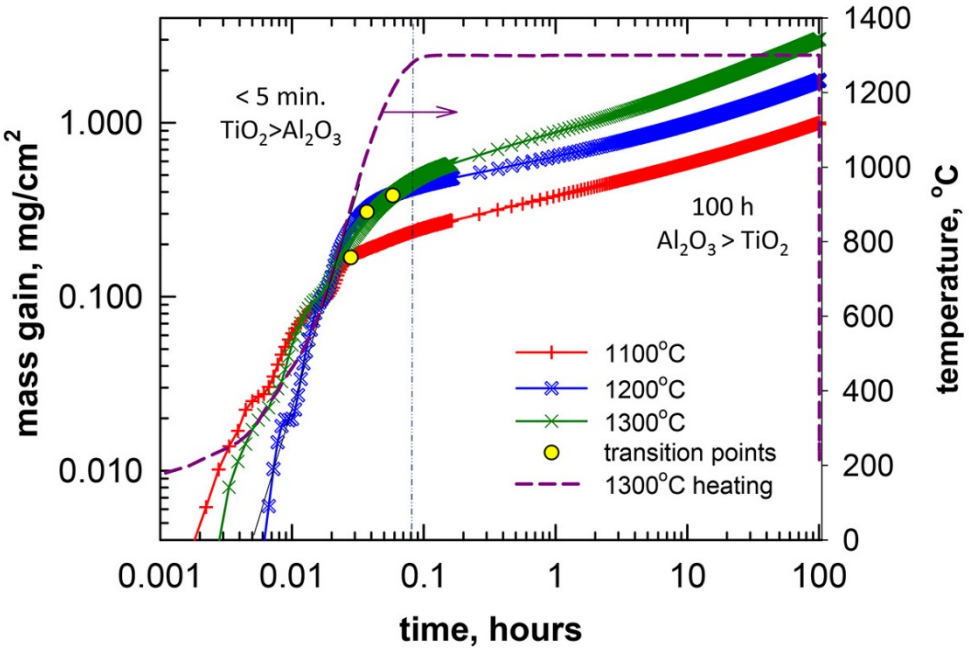

Figure 1.—Transition 'knee' on heating indicate high relative levels of initial transient TiO_2 scale formation on Ti_2AlC during TGA tests (Ref. 9).

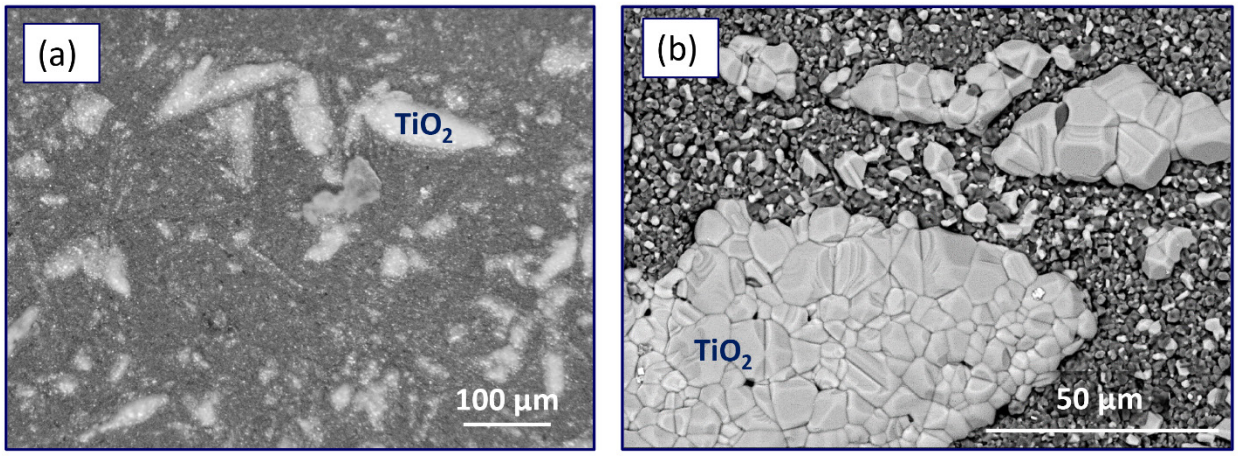

Figure 2.—Transient 'light' TiO_2 surface oxides on Ti_2AlC (Ref. 10). (a) Clusters after 5 min heating to 1300 °C in TGA (optical, 100x). (b) Well-defined TiO_2 crystal colonies after 100 h at 1200 °C in TGA (SEM/BSE, 1000x).

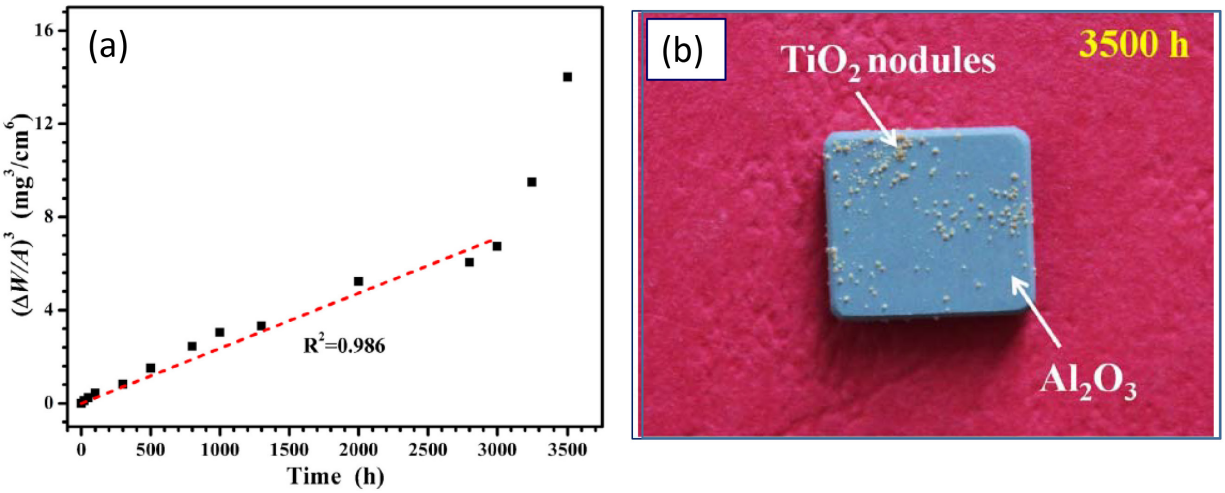

Figure 3.—Long term oxidation of Ti_3AlC_2 at 1100 °C (Ref. 13). (a) Breakaway from cubic kinetics after 3000 h. (b) Initial distribution of damaging TiO_2 nodules at 3500 h. Copyright Corr. Sci., Elsevier; used with permission.

The same authors show that breakaway occurs at 1100 °C even more quickly (50 h) if the scale is repeatedly polished off each 10 h cycle (Ref. 15). This allows Al to be consumed more rapidly during scale re-growth intervals than by continuous oxidation (Figs. 4(a) (b)). Nothing unusual was exhibited for the first four cycles. The amount of TiO_2 surface scale increased somewhat after the 5th cycle. Next, the weight gain jumped from about 0.2 mg/cm^2 after each of the first five cycles to 40 mg/cm^2 after the 6th cycle. Here, the kinetics changed from protective cubic to non-protective linear. This was accompanied by the scale changing from ~2 μm of Al_2O_3 to ~300 μm of layered mixtures of Al_2O_3 and TiO_2. TEM structures after the 6th cycle indicated steady state growth of non-protective mixed oxide scales in contact with an Al-depleted zone on the order of 1 μm. For these experiments, the critical Al content after the 5th cycle, now measured as ~0.97/3, was somewhat more restrictive than breakaway during continuous oxidation. Interestingly, no scale spallation was triggered by this phenomenon because of the excellent thermal expansion match between Ti_3AlC_2 and Al_2O_3.

In a more typical example, extreme temperatures 1600 to 1800 °C have been shown to transition the oxidation reaction from $Al_2O_3/TiAl_2O_5$ protective layers to thick, cracked, non-protective mixed oxide layers accompanied by dissociation to TiC and TiAl (Ref. 16).

The reduction in Al content and outward flux needed to sustain Al_2O_3 growth has been discussed as both a thermodynamic and kinetic requirement for oxidation resistant metallic substrates. Here very low levels (<1 at.%) are generally needed for the thermodynamic requirement for Ni, Fe, or Co-based alloys (Ref. 17). Still, at much higher levels, internal oxidation of Al is known to persist, eventually resulting in non-protective base alloy oxidation or mixed oxide MAl_2O_4 spinels. For Ti-Al alloys, TiO_2 is more stable than the base metal oxides, and the thermodynamic level is much higher, near 50 at.%, (Ref. 18) However protective external layers do not form until the $TiAl_3$ compound composition is approached (Ref. 19). Lower Al content alloys/compounds are susceptible to internal oxygen solution and non-protective mixed scales. Given that TiO_2 formed on lower Ti-Al alloys and that Ti-MAX phases are susceptible to initial transient TiO_2 scales, it is not unreasonable to endorse breakaway mechanisms based on insufficient Al content and supply. As with most alloys and compounds, there is a temperature limit wherein for various reasons a single protective oxide layer cannot be maintained. Once the base element starts to oxidize in a steady state mechanism, rapid consumption of the entire substrate is common.

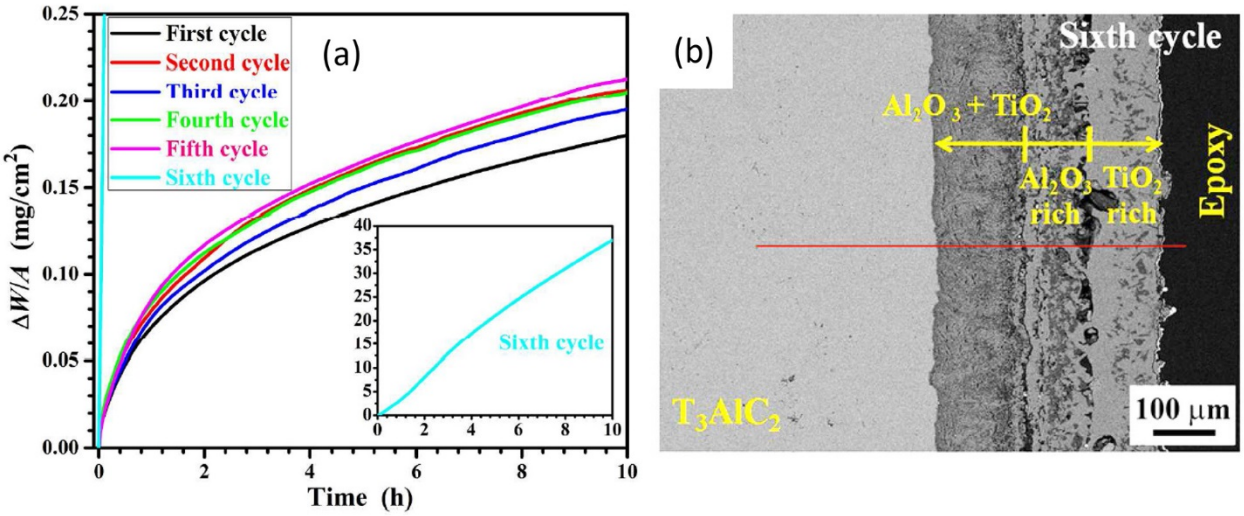

Figure 4.—Effect of repeated oxidation/repolishing cycles (Ref. 15). (a) Oxidation kinetics transformed after five 10 h cycles at 1100 °C. (b) Thick mixed TiO_2/Al_2O_3 layered scale after 6th cycle.
Copyright J. Eur.Cer.Soc., Elsevier; used with permission.

Local Damage in Ti_2AlC

Spot Welds

Less well-recognized is the observation that any coarse surface damage will greatly exacerbate these problems. Rough machining/grinding, impact, indentations, spot welding, EDM, etc. could lead to immediate TiO_2 breakaway. This problem first came to our attention while spot welding Ti_2AlC substrates to a mounting plate for TBC coating in a PS-PVD vacuum chamber (operated by B. Harder). It was found that some spot welds led to uncontrolled TiO_2 nodule growth and rapid sample consumption at moderately high 1200 °C temperatures (Fig. 5). These resulted in huge mass gains as thick breakaway oxidation nodules of TiO_2 overgrew the sample, (Fig. 5(b)). Re-polishing after 5 h did not eliminate the problem upon re-oxidation. A second sample produced similar results with less extensive weight gain (triangles).

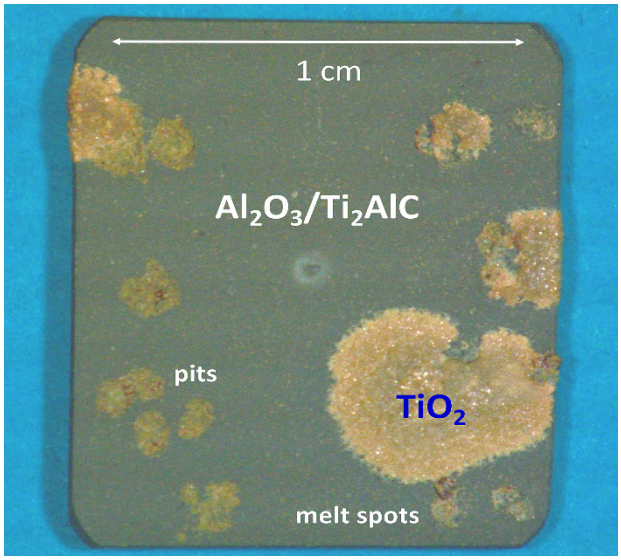

(a)

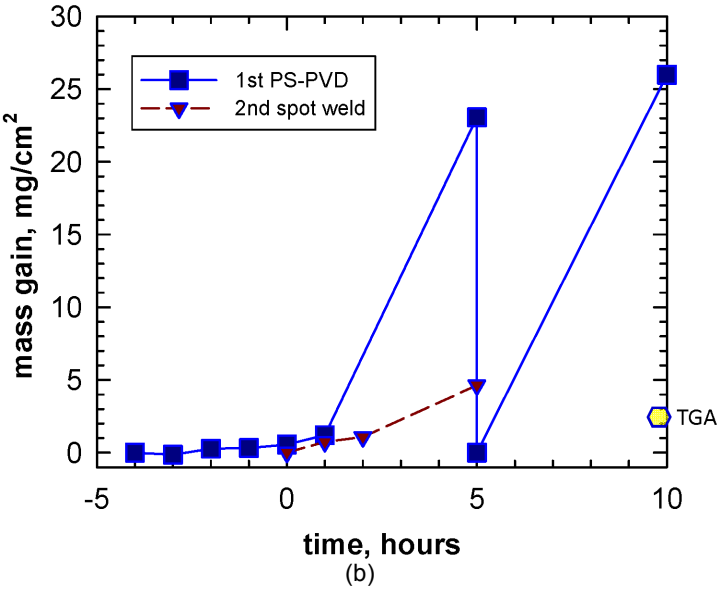

(b)

Figure 5.—(a) Ti_2AlC spotweld damage after 5 h furnace oxidation at 1200 °C. TiO_2 overgrowths, melt spots, and pits. (b) Mass gain for Ti_2AlC spotweld damage after furnace oxidation at 1200 °C from TiO_2 overgrowths; two sample results compared to conventional TGA result.

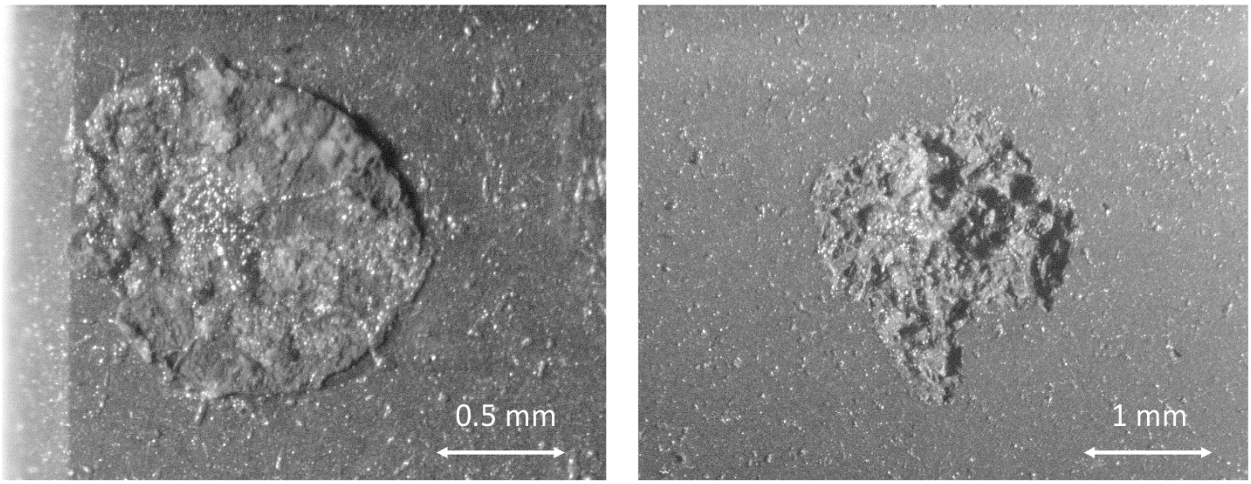

Figure 6.—Details of Ti_2AlC spotweld damage after 5 h furnace oxidation at 1200 °C. melt spots (50x) and pits (25x).

The minimal 10 h results from a TGA run is presented for comparison. Other spots exhibited minor surface melting or cratering, but not necessarily with any loss of Al. Low power spot welds did not necessarily eliminate the problem. (Fig. 6). At this point it was not clear if the high temperature welding event or mechanical damage was the primary factor in causing breakaway oxidation, but the amount of TiO_2 nodulation could greatly exceed the area of initial damage and lead to excessive consumption. The normalized weight gain was 4.6 mg/cm^2 after 5 h. A sister sample was observed for successive 1 h oxidation exposures at nominally 800, 900, 1000, and 1100 °C each, accumulating less than 0.3 mg/cm^2 in total. However, at 1200 °C breakaway oxidation ensued, accruing 0.6, 13, and 27 mg/cm^2 after 1, 5, and 10 h, and nearly total consumption after 30 h when the test was stopped.

The mechanical damage aspect of the spot weld sensitivity was further investigated by using a steel stamping punch and hammer. Various indents were produced in Ti_2AlC oxidation coupons. The oxidation results show again that these sites initiated TiO_2 nodulation upon exposure to 1200 °C in about 1 h. Some expansion of TiO_2 colonies can be discerned over the next 50 h, but not all-consuming Figure 7. In addition, scratching with a diamond stylus by hand, at various pressures, produced TiO_2 nodulation at the scratch to various degrees. TiO_2 growth from 1 to 50 h is again seen to be slow and not all-consuming, Figure 8.

To show the thermal aspect of the damage, a corner of a coupon was impinged by an oxy-acetylene torch flame for about a minute. These typically induce temperatures in the 2000 °C range for softening sapphire (Al_2O_3) rods, so it is logical to assume the Ti_2AlC max phase approached its dissociation temperatures (somewhere above ~1500 °C). The initially sharp corner was observed to glow and deform into a rounded bead-like shape. But subsequent oxidation at 1200 °C showed little expansion of TiO_2 nodulation originating from this site, Figure 9.

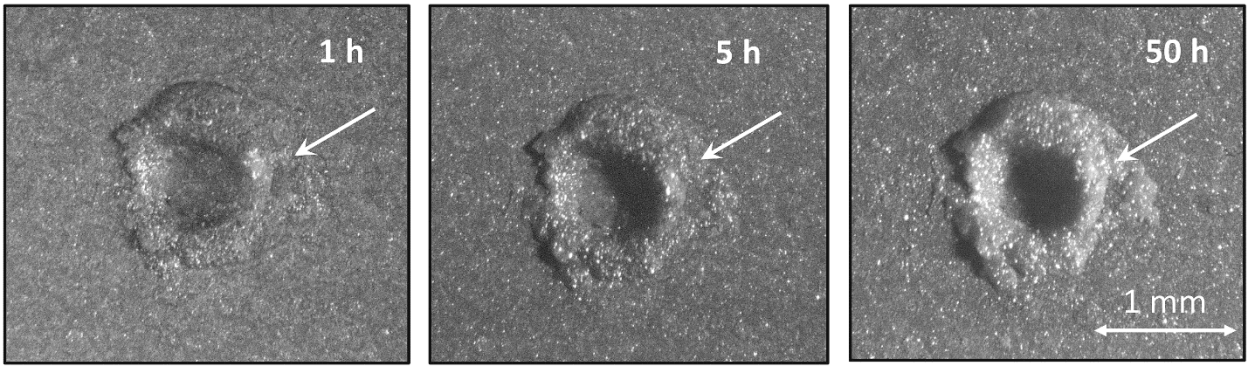

Figure 7.—TiO_2 overgrowth at area damaged by a metal punch. After 1, 5, 50 h at 1200 °C.

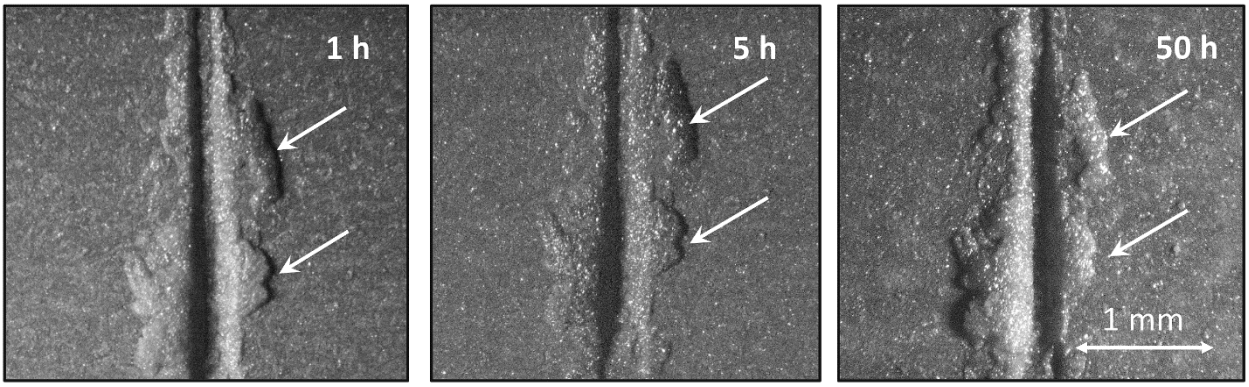

Figure 8.—TiO_2 overgrowth at scratch from a diamond stylus. After 1, 5, 50 h at 1200 °C.

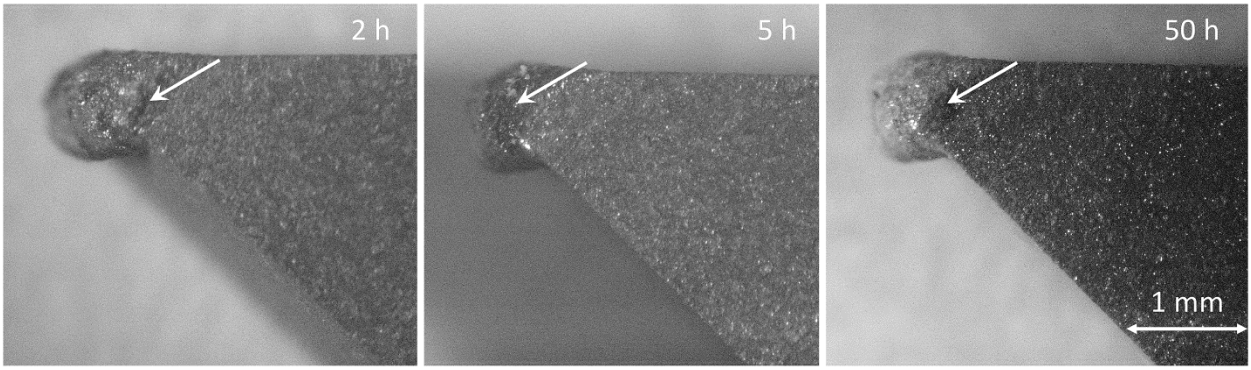

Figure 9.—TiO_2 overgrowth at area melted by an oxy-acetylene torch. After 2, 5, 50 h at 1200 °C.

EDM and Surface Finish

Small 1 cm square by 0.4 mm thick spacers, used for burner rig sample attachment fixtures, were EDM machined from the parent ingot of MAXthal 211™ (Fig. 10). They were then subjected to 6 atm, 30 m/s HPBR exposures at about 1482 °C (2700 °F), as controlled by the EBC-coated CMC disk sample temperature. After one 6 h exposure, the spacers were completely oxidized, exhibiting the tell-tale white color of the TiO_2 external surface. Many were largely consumed and missing after the test. The remaining were all broken from oxidative growth stresses while under the mechanical constraint of the oxidized bolts. Cross-sections of salvaged spacers indicated a mixed-oxide shell, with variable amounts of original Ti_2AlC remaining at the core (Figs. 11 and 12). This consumption was likely caused by excessive temperatures. The oxidative degradation of the attachment bolts contributed to more chemical attack and breakage upon removal.

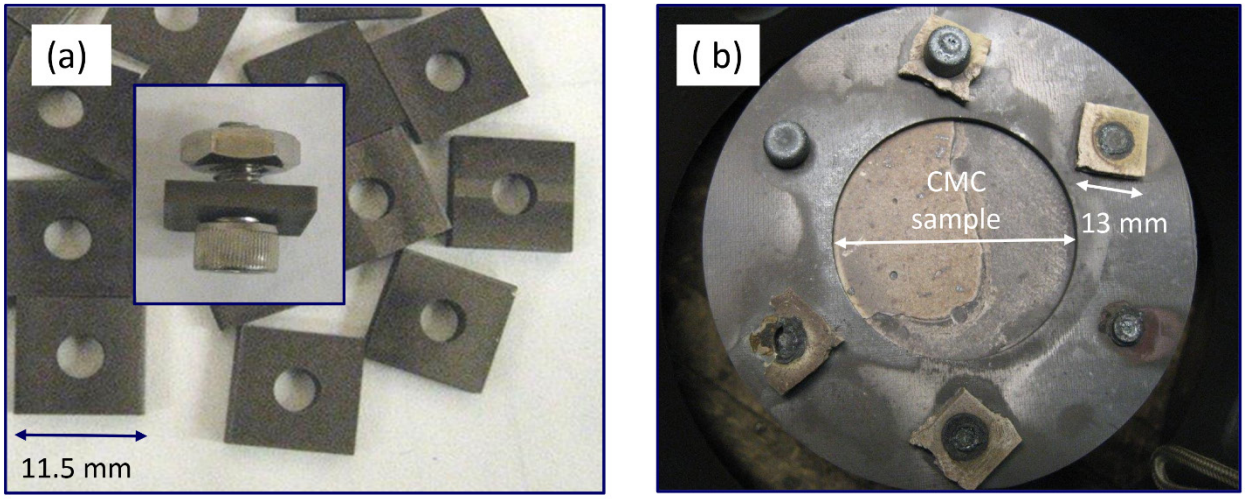

Figure 10.—EDM'd Ti2AlC MAXthal bolt spacers for HPBR attachment. (a) As-machined; (b) Fixtured mounting plate: exposed and heavily oxidized in HPBR at Tgas ~1482 °C, 6 h.

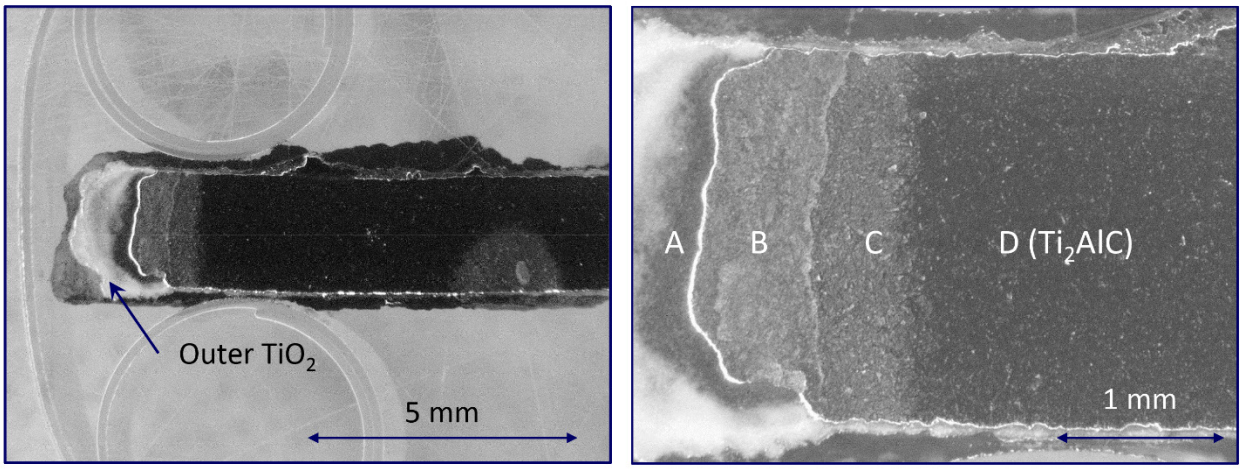

Figure 11.—Polished edge-on view of Ti_2AlC spacer from (Fig. 10(b)) showing four distinct oxidation zones and substrate (D).

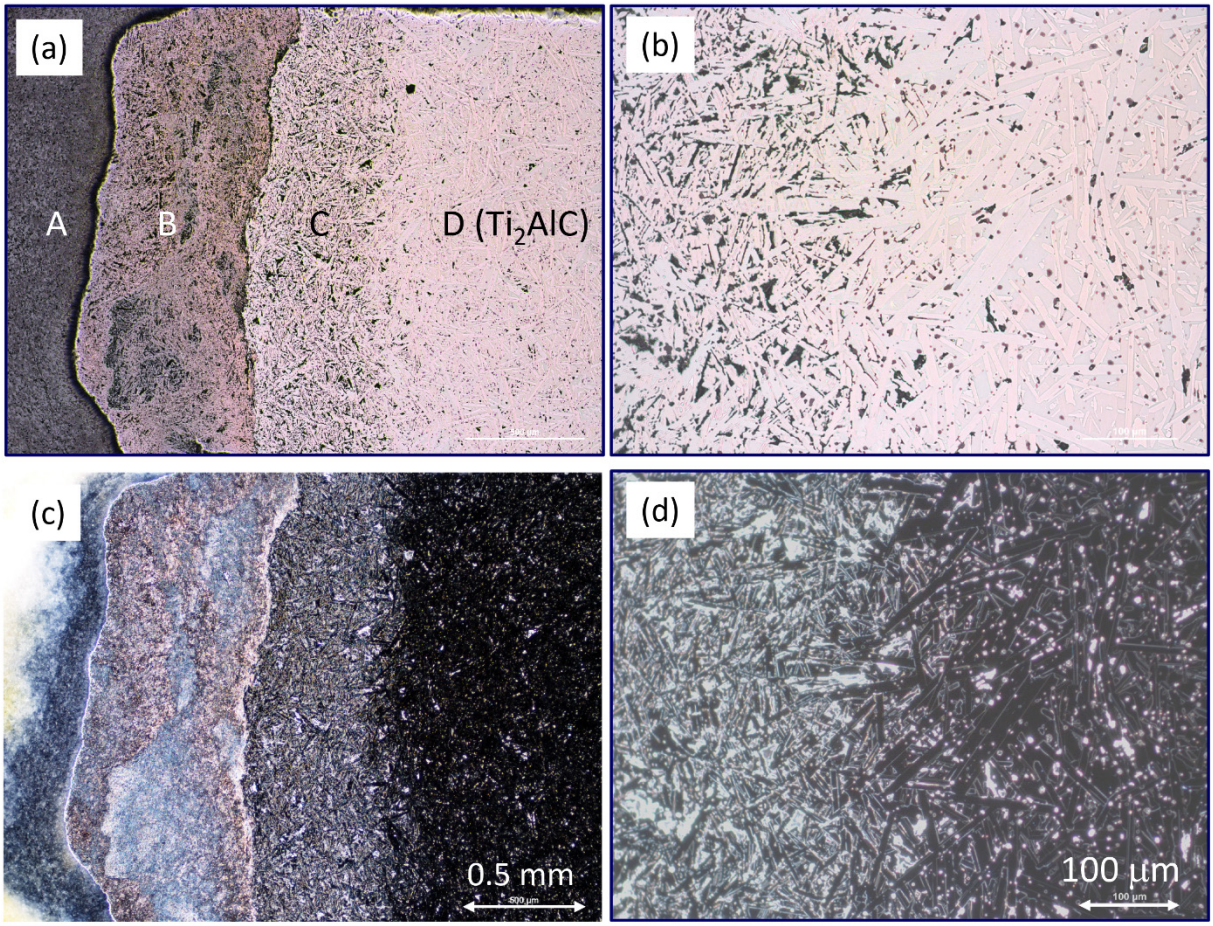

Figure 12.—Details of oxidation layers in Figure 11. (a) distinct layers; (b) Ti_2AlC lathes and dark inclusions in layer C; (c,d) dark field of (a,b) showing extensive bright oxide corresponding to dark inclusions above.

To study any effects of EDM machining, fresh Ti_2AlC spacers were oxidized in static air at 1200 °C up to 50 h. One face and edge were polished to 2400 grit emery. Other edges were sanded to 180, 325, and 600 grit. It can be seen that TiO_2 selective degradation is associated with one side and one edge (Fig. 13). Thus some aspect of the spark cutting may have initiated chemical dissociation or basal plane separations in the MAX phase structure and triggered TiO_2 runaway oxidation. Polishing the edges to 180 grit did not fully eliminate the tell-tail yellow TiO_2 scale appearance; 325 grit was partially transitioned with less TiO_2, and 600 grit polishing fully changed the oxidized surface to gray Al_2O_3. Al_2O_3 was also produced on the major face polished to 2400 grit (Fig. 14). It is interesting that the degradation appeared to progress only part way from the edge on one side, then appeared to stabilize after just 1 h.

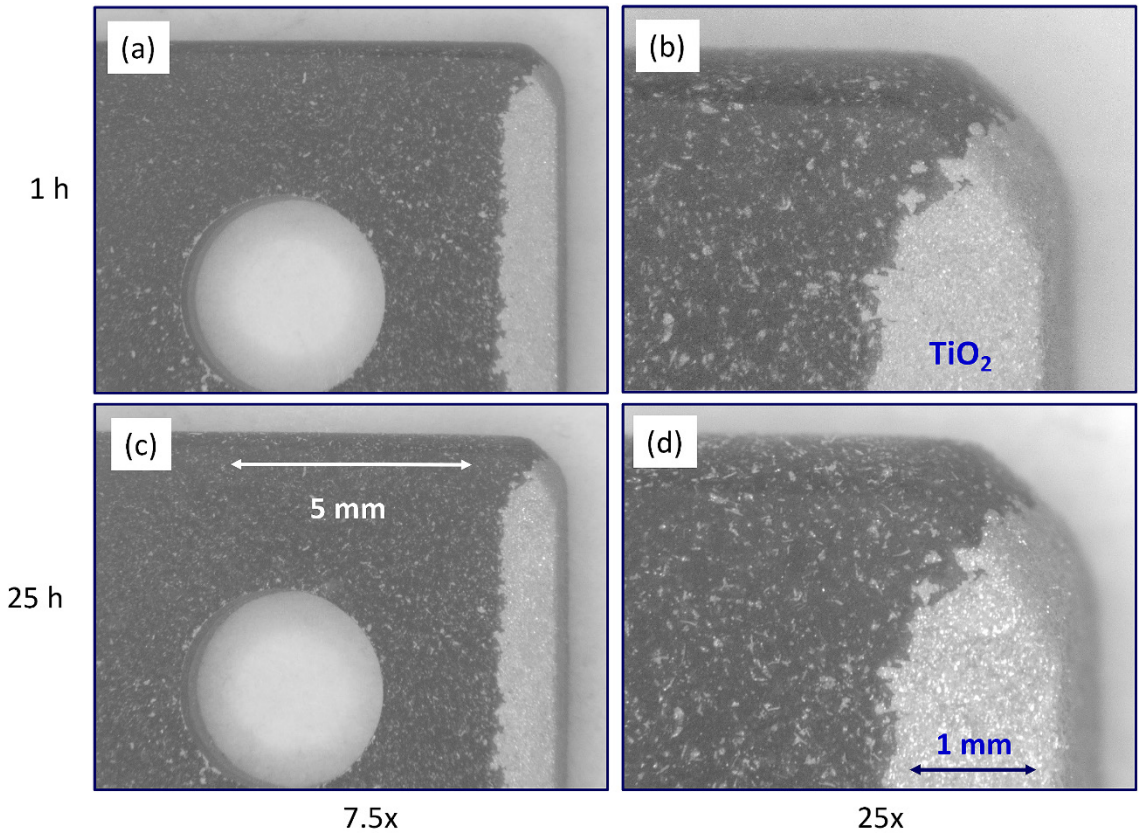

Figure 13.—Ti_2AlC EDM'd spacer after furnace oxidation at 1200 °C. (a,b) TiO_2 overgrowth after 1 h; (c,d) stabilized to 25 h (7.5x, 25x).

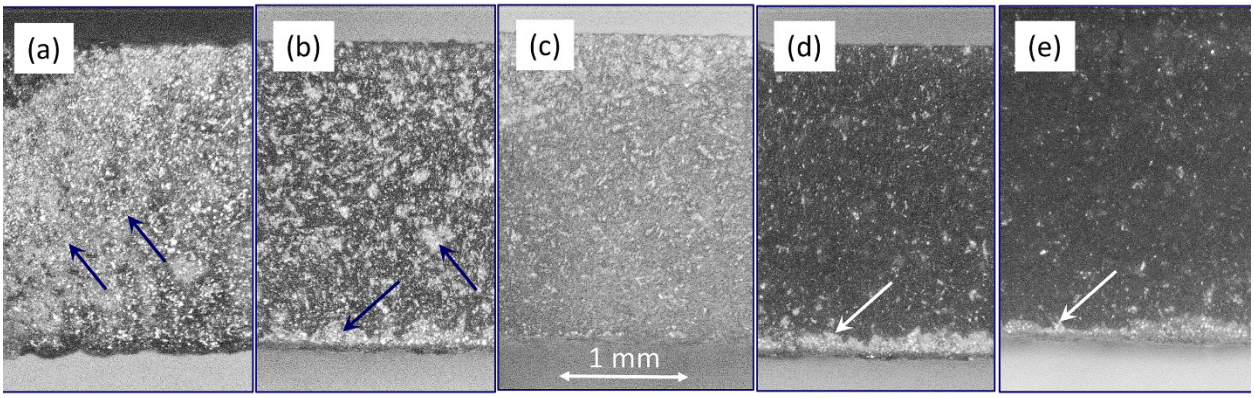

Figure 14.—Ti_2AlC spacer surface after 50 h furnace oxidation at 1200 °C. Bright TiO_2 features for (a) EDM, (b) 180, (c) 325, (d) 600, and (e) 2400 grit (25x). Arrows point to dense TiO_2 overgrowth on EDM and 180 grit surfaces.

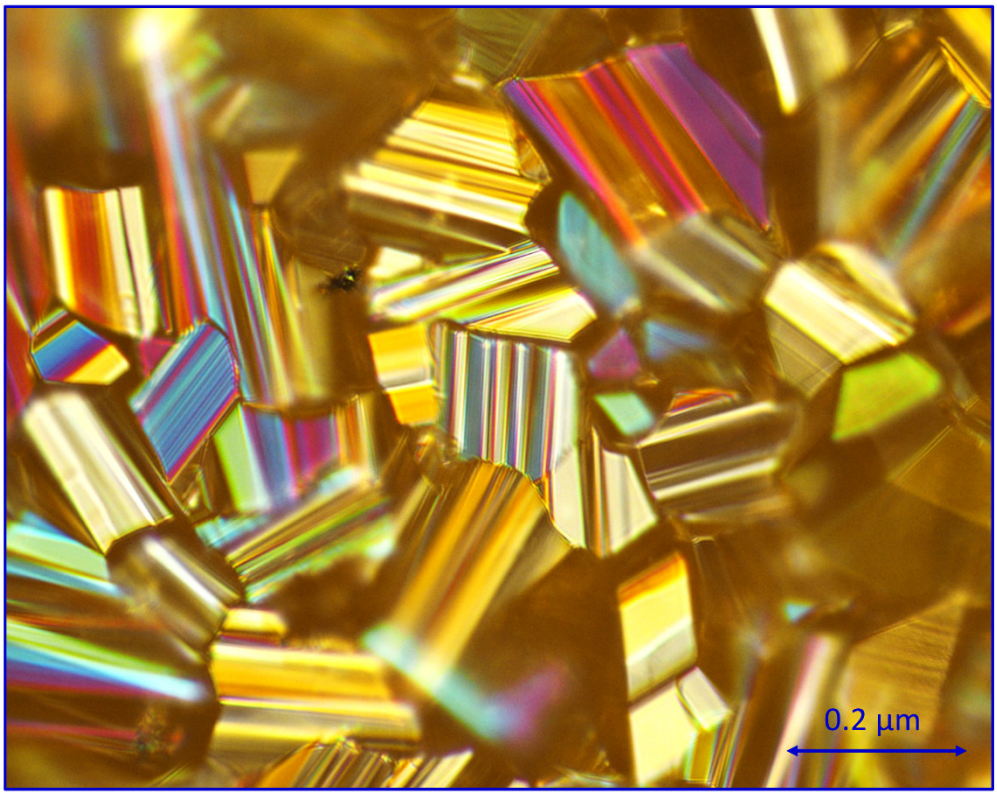

Figure 15.—Heavily twinned structure revealed by crossed polarized light microscopy. TiO_2 overgrowths for EDM'd Ti_2AlC spacer after 50 h furnace oxidation at 1200 °C.

The TiO_2 structure on the surface of the as-EDM-machined Ti_2AlC surface was that of large impressive faceted TiO_2 rutile crystals, as often associated with oxidation of Ti-rich materials (Refs. 19 and 20). The structure appears to be that of twinned crystals in the optical color micrograph of the surface obtained with crossed polarizers, Figure 15. In summary, surface damage or finish appears to influence the amount of transient TiO_2 that forms before a healing underlayer of Al_2O_3 forms, depending on the degree of damage. However, this did not necessarily transition into runaway TiO_2 growth and consumption of the substrate as occurs in true breakaway oxidation.

Scale Volatility on Ti_2AlC

For the most part, the presence of water vapor in the environment did not influence the scale phases or growth kinetics. However, some indication of moisture-assisted scale volatility was presented in Reference 21 and explained as $TiO(OH)_2$ formation that had been identified by (Ref. 22). Furthermore, volatility of Ti-surface oxides has been discussed in burner rig testing of Ti_2AlC and water vapor effects (Ref. 10). It appeared that TiO_2 and $TiAl_2O_5$ surface scales could be removed by H_2O with the formation of volatile $TiO(OH)_2$ species, but nowhere near the rate of Al_2O_3 scale growth. This would therefore not be considered life limiting. The volatility rate could only be conclusively quantified by burner rig testing of a heavily pre-oxidized sample to the low value of –0.012 mg/cm^2/h Figure 16. Prior to burner rig testing, the surface microstructure exhibited primarily $TiAl_2O_5$ and TiO_2 covering a base layer of Al_2O_3. After the test, the remaining surface was primarily Al_2O_3, Figure 17. However, for the protective Al_2O_3 scales, volatility did not appear to be severe and, again, would not be considered a critical factor for turbine environments at 1300 °C and below.

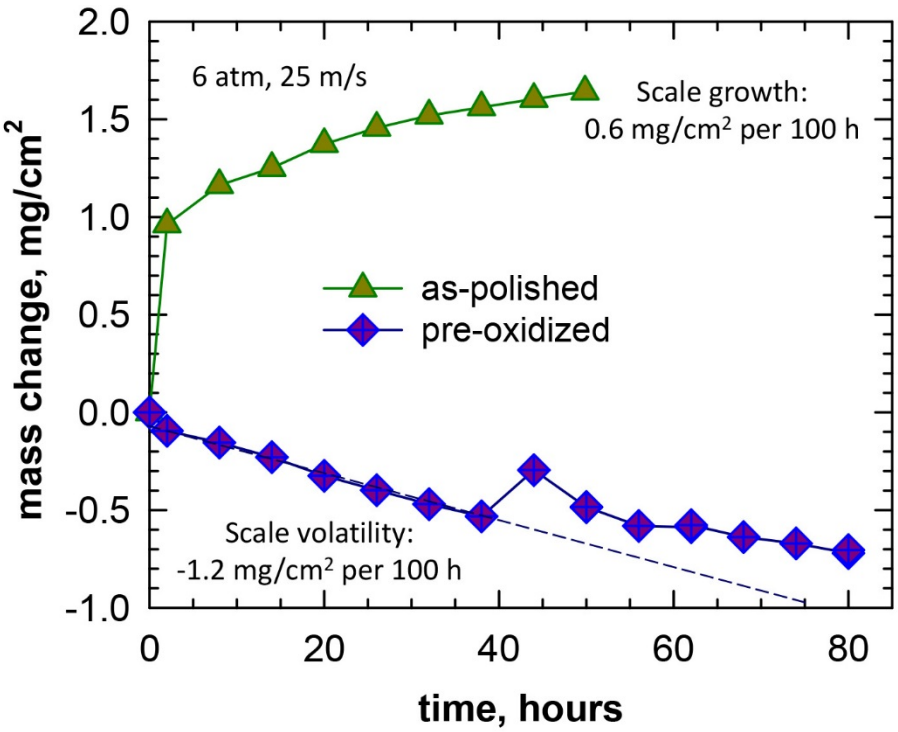

Figure 16.—Weight loss for pre-oxidized Ti_2AlC in 1300 °C high pressure burner test. Loss is masked by higher initial rates of oxidation (as-polished) (Ref. 10). Copyright J. Eur.Cer.Soc., Elsevier; used with permission.

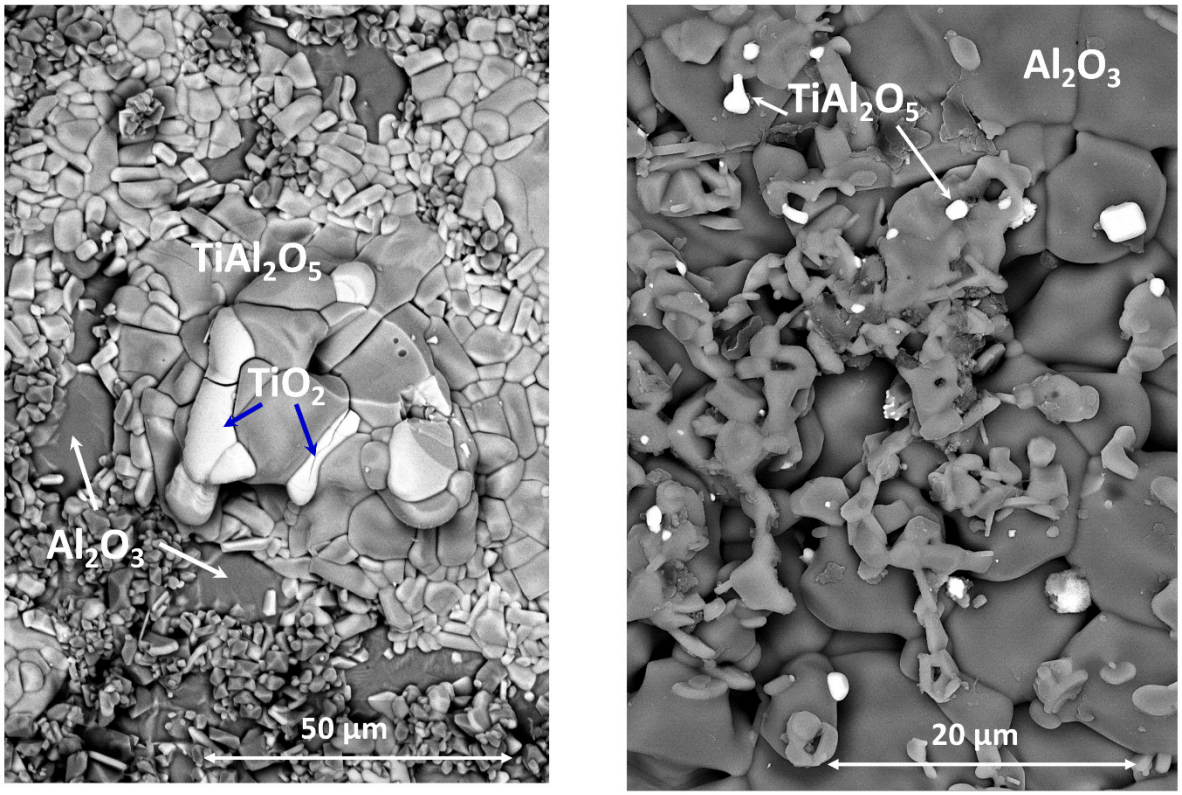

Figure 17.—Ti-rich scale features atop an Al_2O_3 scale on formed on Ti_2AlC at 1300 °C (SEM/BSE). (a) after furnace pre-oxidation for 300 h; (b) removed by subsequent 50 h exposure in HPBR (Ref. 10). Copyright J. Eur.Cer.Soc., Elsevier; used with permission.

Cr_2AlC Issues

Isothermal Oxidation

In general, it is found that oxidation of Cr_2AlC follows the same (cubic) kinetics as the Ti-Al-C MAX phases (Refs. 2, 7, and 23). However, occasionally it has been found that Cr_2AlC samples exhibit anomalous weight losses in TGA tests at 1200 °C and above, Figure 18 (Ref. 24). In our own 1200 °C tests, we have found continuous TGA curves to vary with the material/manufacturer, Figure 19. Here various levels of a second phase Cr_7C_3 were found by metallography, as exemplified by the microstructure in Figure 20 (Ref. 25). The amounts determined by Rietveld analyses of XRD diffractometer scans were 6.8, 2.8, (varying from 1.6 to 4.2% optically) and 0.0 vol% for the samples obtained from Kanthal, Drexel/312 (M. Barsoum), and Delft Univ. (W. Sloof), respectively. It can be seen that the higher loss rates follow to some extent with higher Cr_7C_3 amounts, finally showing no visible losses for the highest purity Cr_2AlC (Delft). Furthermore, it was shown for the Kanthal material that the Cr_7C_3 phases oxidized to Cr_2O_3 at 800 °C (Ref. 26). Thus, at high temperatures (or in water vapor), volatile CrO_3 (or $CrO_2(OH)_2$) species can be expected to contribute to mass losses in isothermal tests and an accelerated degradation mechanism. Apparently, prevention of this phase is a troublesome practical processing problem to be overcome to achieve the optimum and broadest performance of this compound.

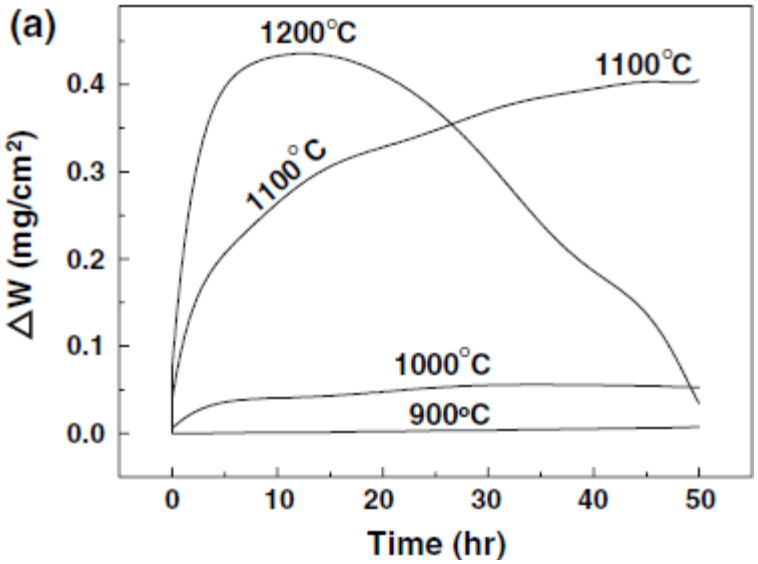

Figure 18.—Isothermal oxidation of Cr_2AlC. Modest weight gains from 900 to 1100 °C, but weight losses after 10 h at 1200 °C (Ref. 24). Copyright Oxid.Met., Springer; used with permission.

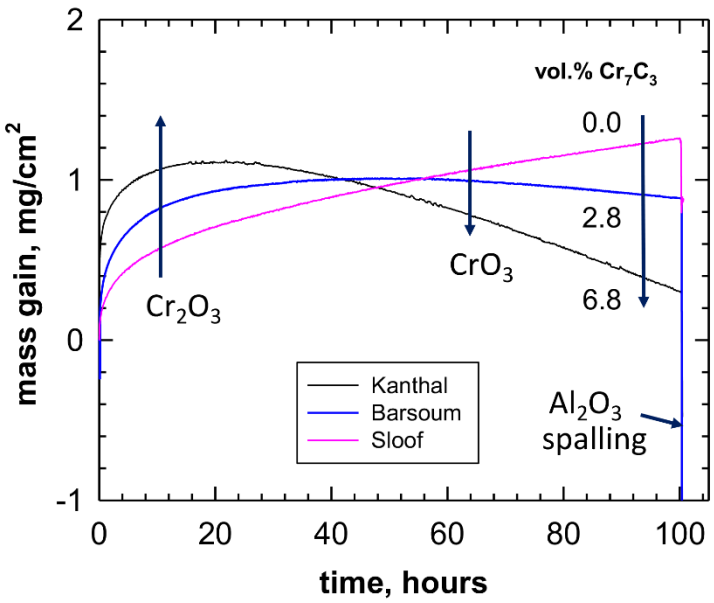

Figure 19.—1200 °C Isothermal oxidation of various Cr_2AlC materials. Weight losses may occur with time. (unpublished data, Smialek, from 2015).

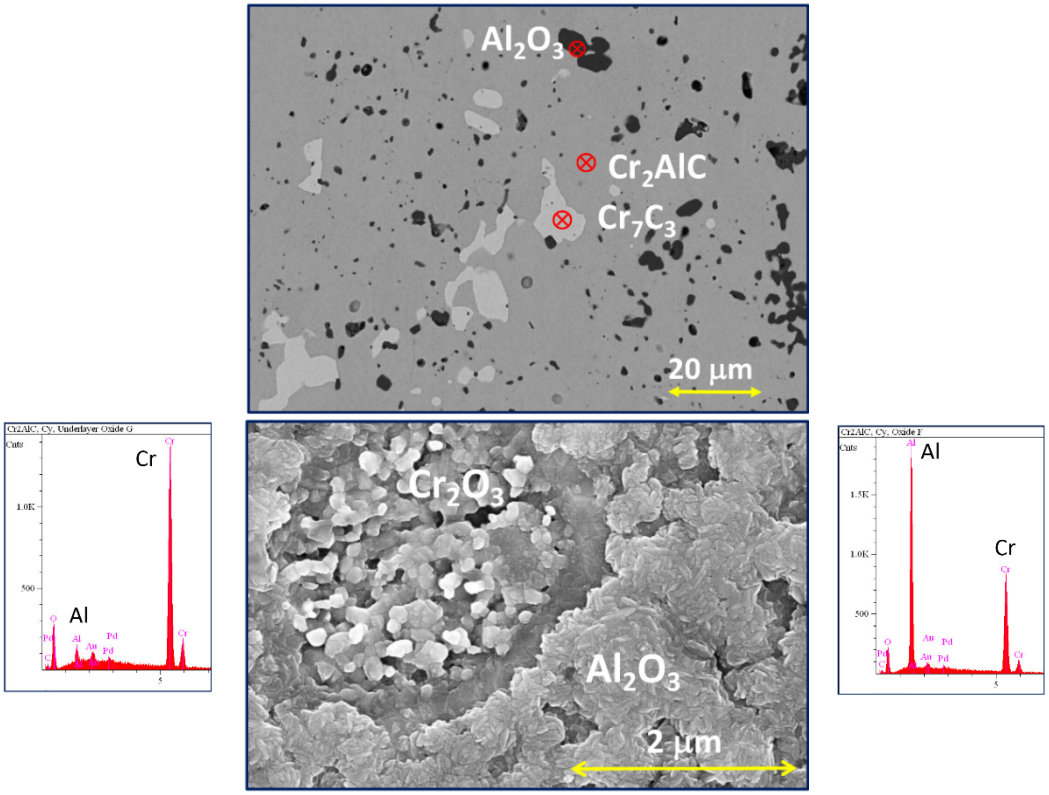

Figure 20.—Cr_7C_3 second phase particles in (a) polished Cr_2AlC (Kanthal) cross section sample and (b) selective Cr_2O_3 surface scales formed over similar regions. Hot pressed 1100 °C/2 h and oxidized 800 °C/100 h (Ref. 26).

Scale Adhesion

It is widely demonstrated that Al_2O_3 scale adhesion is a problem for Cr_2AlC, showing many instances of scale removal to a bare, transformed ceramic surface. This exposed surface is generally observed to consist of a Cr_7C_3 depletion zone. Re-oxidation of this phase produces less protective Cr_2O_3 or mixed scales, among other problems such as interface porosity. Cyclic oxidation tests have demonstrated that this scale adhesion problem exists at 1200 °C and above, Figure 21. Cycling also produces layered scales, as repeated spallation further depletes the compound of Al and allows Cr_2O_3 formation. Spallation also occurs after isothermal tests that formed a relatively pure Al_2O_3 layer, revealing the Cr_7C_3 depletion zone with telltale imprints of the Al_2O_3 grains, Figure 22 (Refs. 24, 27, and 28).

This behavior and interface structure are very reminiscent of non-adherent scales formed on undoped NiAl and MCrAl alumina-forming alloys (Refs. 29 and 30). Here the interface bond weakness and eventually porosity encourage interfacial spallation upon cooling. For decades the oxidation resistant alloys relied upon reactive element doping to improve scale adhesion. One first order effect of the reactive elements was to prevent interfacial sulfur segregation and bond weakening (Ref. 31). Following this logic, adherent scales were produced without dopants by removing sulfur from the alloy.

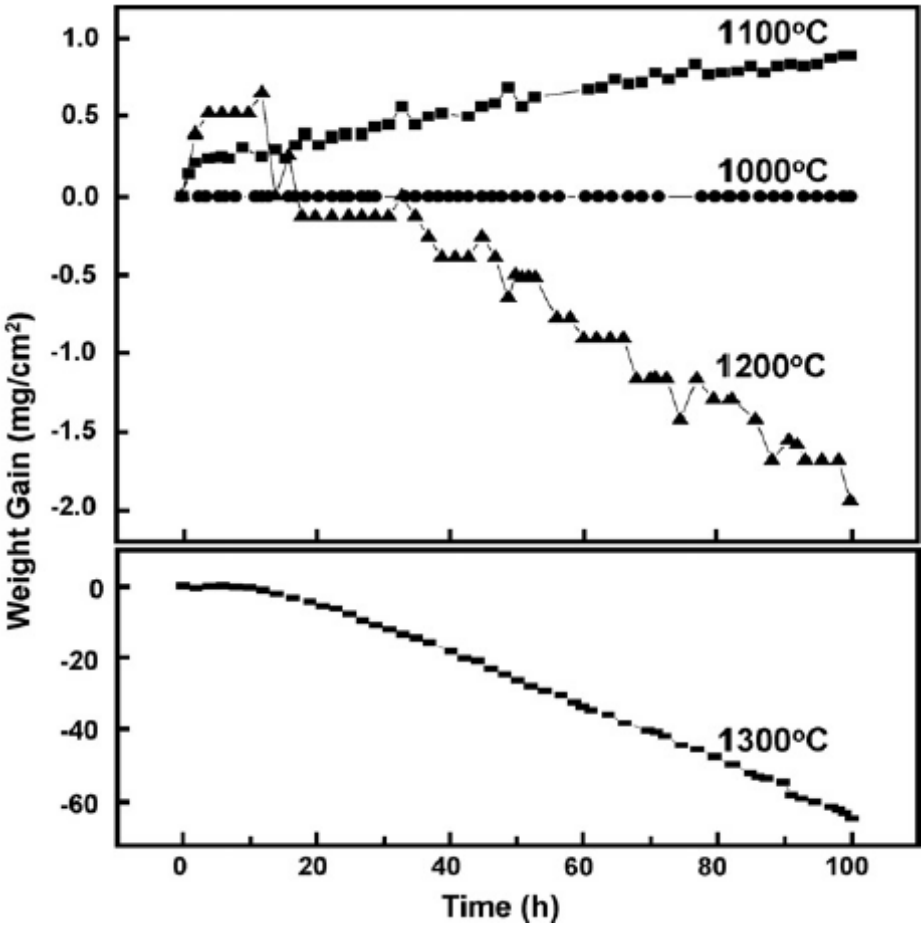

Figure 21.—Temperature effects on cyclic oxidation weight change curves for Cr_2AlC. 2 h cycle in air (Ref. 32). Copyright J.Alloys.Comp., Elsevier; used with permission.

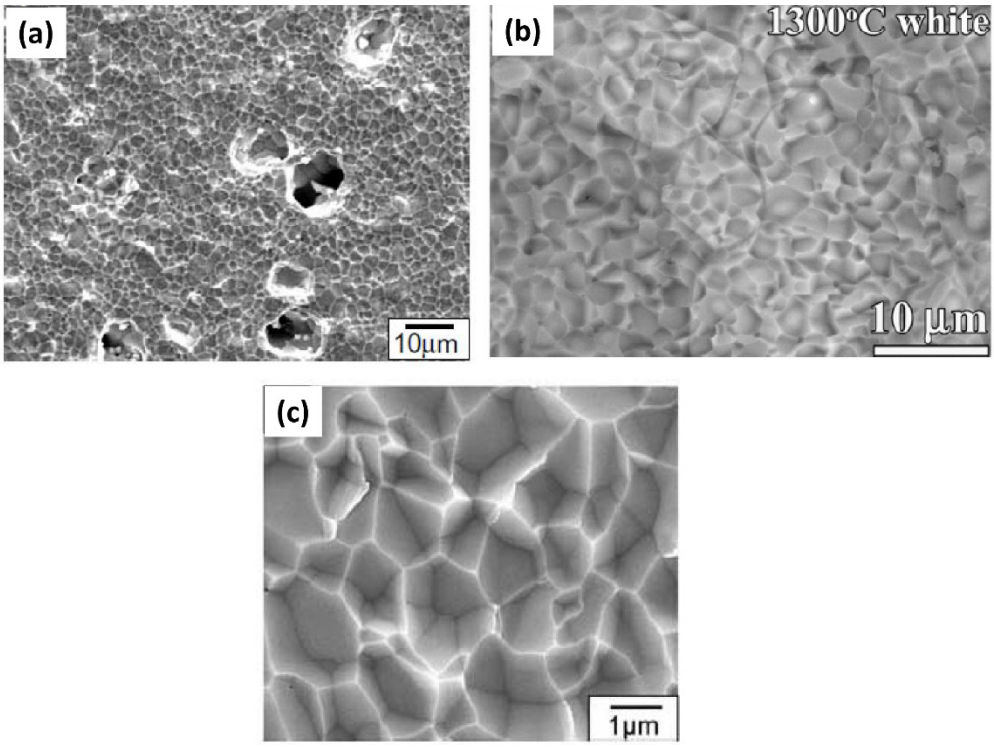

Figure 22.—Cr_7C_3 interface in Cr_2AlC exposed by Al_2O_3 spallation after isothermal oxidation in air. Oxide grain imprints and porosity. (a) 1300 °C, 100 h, (Ref. 27) Copyright Corr. Sci., Elsevier. (b) 1300 °C, 20 h, (Ref. 28) Copyright Acta mat., Elsevier. (c) 1100 C/480 h, (Ref. 24) Copyright Oxid.Met., Springer. Images for (a), (b), and (c) are used with permission.

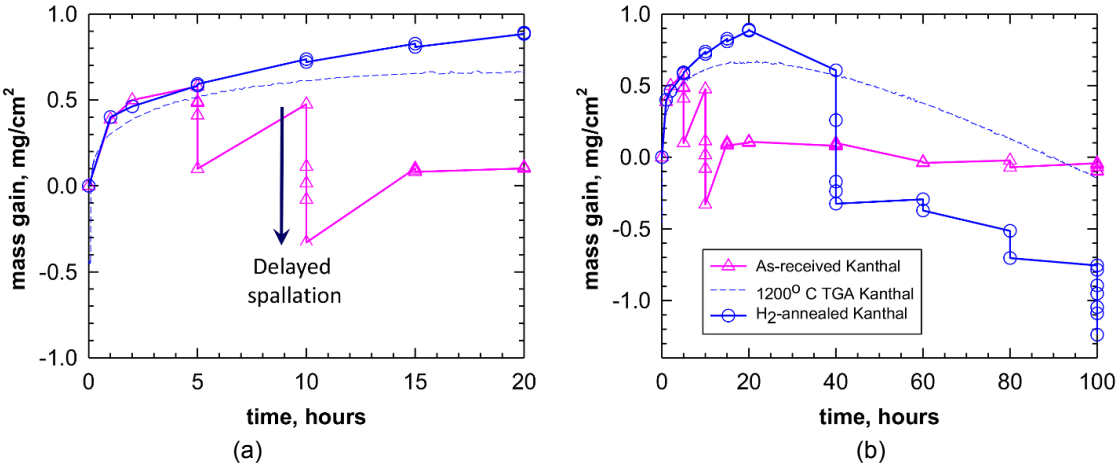

Figure 23.—Intermittent oxidation of Kanthal Cr_2AlC at 1200 °C. (a) Al_2O_3 scale spallation for the as-received sample at 5 and 10 h; no spallation for the H_2-annealed sample for 20 h. (b) subsequent reduced spallation for the as-received sample; but increased spallation at 40 and 100 h for the H_2-annealed sample.

One efficient process to achieve this was by hydrogen annealing ≥1200 °C (Ref. 31). This allowed for surface segregation of sulfur to occur without a scale barrier, leading to gaseous removal of sulfur to produce bulk S levels ≤0.1 ppmw. In that regard, samples of Cr_2AlC were hydrogen annealed by the same process at 1250 °C for 50 h. The first material so treated was pressureless sintered (to 96%) Cr_2AlC obtained from Kanthal, as characterized in Reference 25. Sulfur analyses by GDMS, however, revealed only a decrease from 9.4 ppmw to 7.4 by hydrogen annealing. The samples were then intermittently oxidized and monitored by weight change and appearance. The gravimetric data is shown in Figure 23.

From Figure 23(a) it appears that the H_2 anneal results in scale adhesion, at least up to 20 h. By contrast, the as-received sample, sanded to a 2400 grit emery finish, produced moisture-induced delayed spallation (MIDS) at 5 and 10 h. This is where additional amounts of interfacial spallation occur, well after cool down, due to interactions with ambient humidity. It is documented by successive weight measurements, as exhibited by the distinct vertical drops (losses without reheating/cooling) at a single oxidation time. This phenomenon has been well-documented for Al_2O_3 scales formed on metal substrates (Ref. 30).

A more extensive test was conducted at 1150 °C for 100 h on four Cr_2AlC materials. These materials were the original Kanthal Cr_2AlC, a sintered bar from Prof. M. Barsoum/Drexel U., a hot pressed sputter target ingot from powders produced at Drexel U. (Miller/Barsoum), and a high purity Cr_2AlC sintered sample from Prof. W. Sloof/U. Delft. They all exhibited similar delayed spallation phenomena, Figure 24. Here massive areas of spallation to bare substrate surface occurred, with re-oxidation to a less uniform, Cr-rich scale. Small particle spallation and green CrO_3 - contaminated alumina boats were then observed, as indicated by vapor phase losses in TGA (Fig. 19). It should be noted that these interrupted tests at 1150 °C produced 100 h weight changes in the range of –0.5 to 1.5 mg/cm^2. At 1200 °C the 100 h weight change ranged from –1.3 to 0 mg/cm^2. This compares reasonably close to the 100 h weight change of 0.8 mg/cm^2 at 1100 °C and –2 mg/cm^2 at 1200 °C using 2-h cycles (Ref. 32).

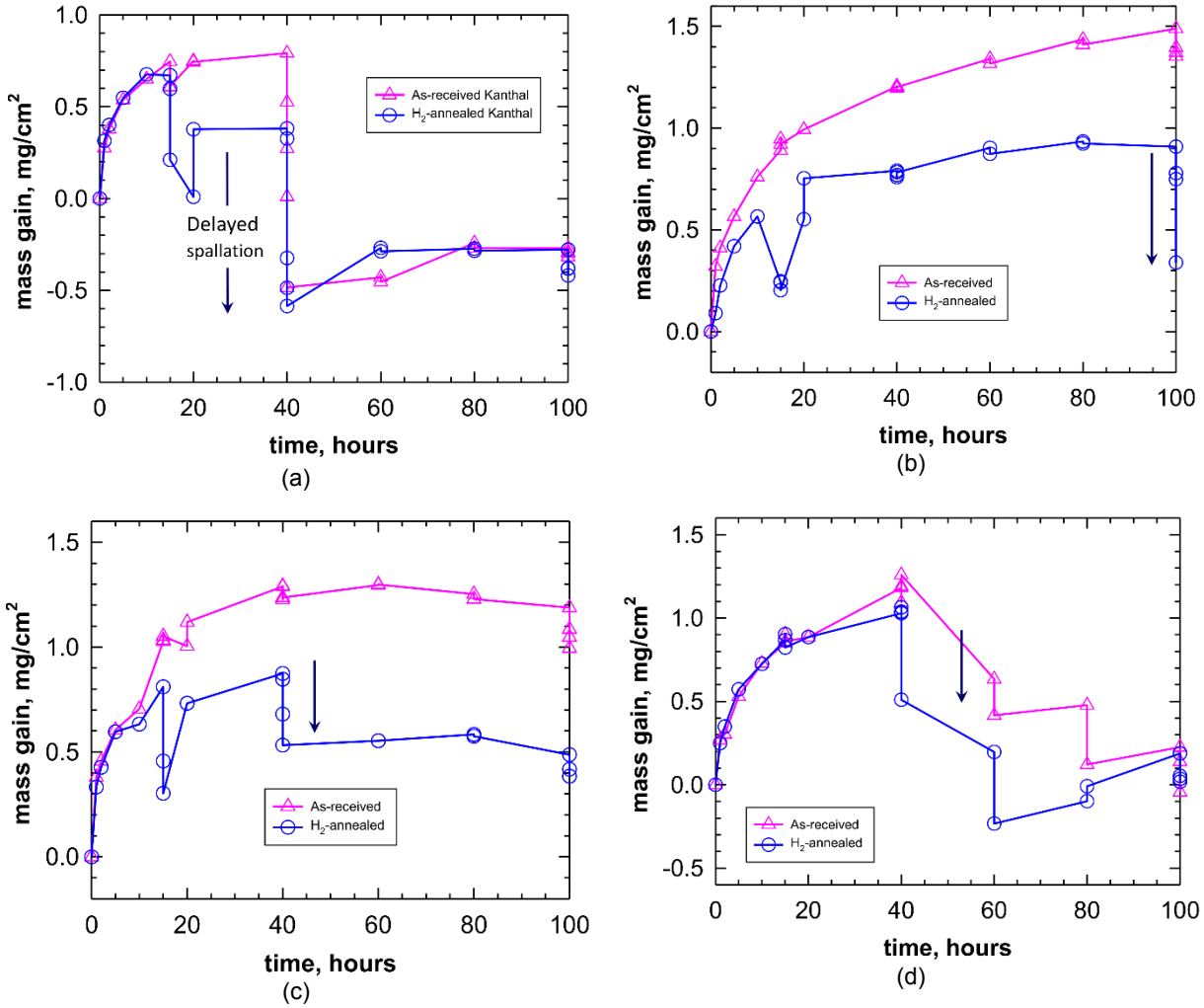

Figure 24.—1150 °C intermittent oxidation of Cr_2AlC showing delayed spallation (vertical drops). (a) Kanthal; (b) Barsoum/Drexel; (c) R.A. Miller/Barsoum; (d) Sloof.

The general surface appearance of these samples is presented in the optical micrographs of Figure 25 after a significant spalling event has occurred. Here the spalled regions are the bright, reflective, exposed textured regions, presumably Cr_7C_3. The texture arises from the grain boundary imprints of the scale left in the Cr_7C_3, cf. Figure 22. Upon scale regrowth over these exposed and Al-depleted regions, a darker appearing scale with only micro-regions of spallation occur. This is believed to be a transition to mixed Al_2O_3-Cr_2O_3 scales with modified kinetics and spallation behavior. XRD analyses of the surface after 100 h oxidation yielded significant levels of α-Al_2O_3, Al_2O_3-Cr_2O_3 solid solution, and Cr_2O_3. Cr_7C_3 was also identified in the as-received oxidized sample, with an increased level in the H_2–annealed sample after oxidation due to the MIDS shown in Figure 23(b). It is curious that the regrown scale on the as-received sample appears to have an uneventful weight change behavior after 20 h, Figure 23(b), although the 100 h surface appearance (not shown here) suggests small iterative spallation events. It is not clear how protective these regrown mixed scales may be in the long term. Clearly there is some difference in these tests, trending to a flat oxidation curve, compared to the typical continuous losses shown in Figure 21 for cyclic oxidation.

Attempts at improving adhesion by hydrogen annealing produced only modest gains in initial scale adhesion and did not prevent interfacial spallation for the long term. Furthermore, the sulfur content, believed to be of prime importance in influencing weak interfaces and scale spallation, did not change appreciably by hydrogen annealing (only ~25% reductions). This is compared to metallic samples that have revealed orders of magnitude reductions in sulfur content (from 10 to 0.1 ppmw S) and commensurate improvements in scale adhesion.

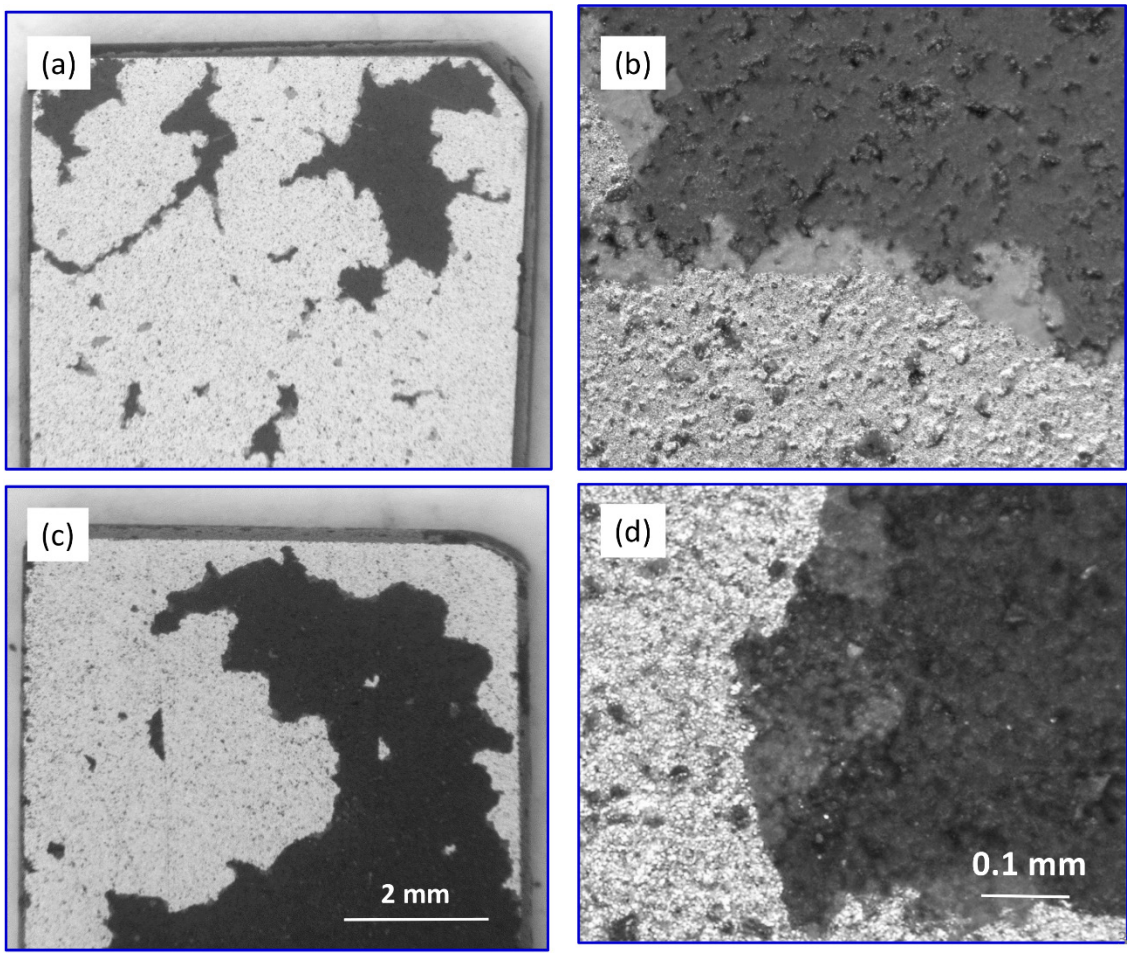

Figure 25.—Al_2O_3 scale spallation after 1200 °C oxidation of Kanthal Cr_2AlC. (a,b) as-received, 5 h. (c,d) H_2 annealed, 40 h. (7.5x, 100x).

The oxidative life of YSZ TBCs on Kanthal Cr_2AlC substrates was tested in an identical manner as those studied for Ti_2AlC substrates. Ti_2AlC substrates enabled survival in stepped temperature tests up to 1300 °C because of an excellent CTE match (Ref. 14). However, the Cr_2AlC substrates began to show interfacial spallation after 400 h at 1150 °C and TBC failure after 100 h at 1200 °C, Figure 26. Here both delayed moisture-induced scale spallation (MIDS) and delayed TBC desk top spallation (DTS) were exhibited. These results are reminiscent of the intermittent oxidation results shown in Figure 24. The stepped oxidation TBC studies, however, accrued test times over 1000 h (and thicker scales) at temperatures below 1200 °C, implying longer durability for those stepped oxidation testing profiles. The onset of these failures, again exhibiting interfacial spallation to the substrate, is exemplified in Figures 27 and 28.

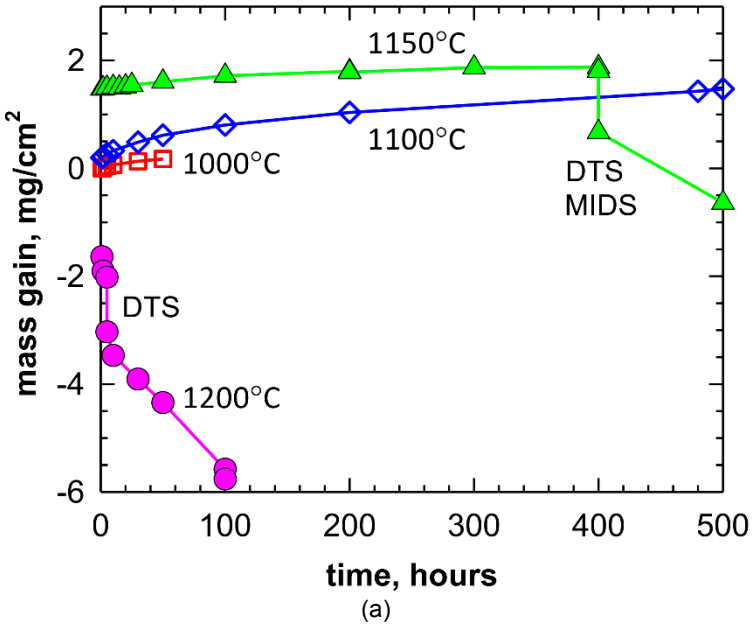

(a)

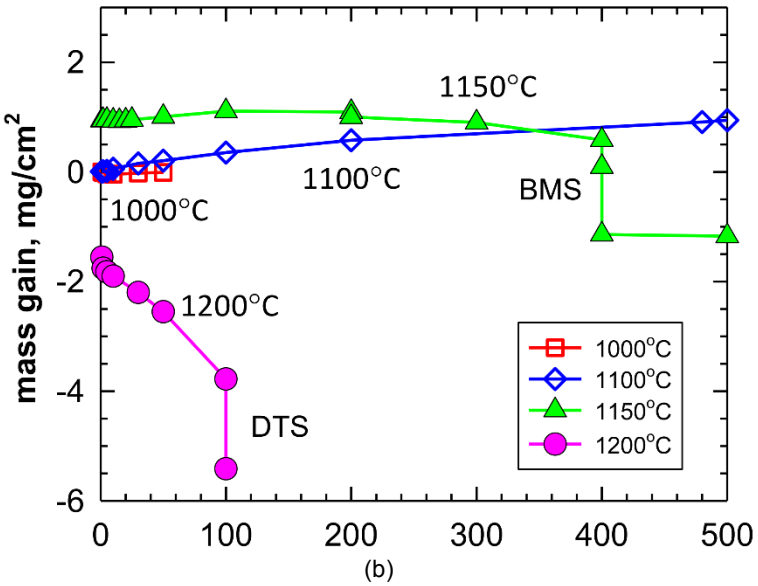

(b)

Figure 26.—Stepped oxidation response for YSZ thermal barrier coating on Kanthal Cr_2AlC. Scale (MIDS) and TBC (DTS) failure initiated at 1150 °C and terminated at 1200 °C. (a) APS, (b) PS-PVD.

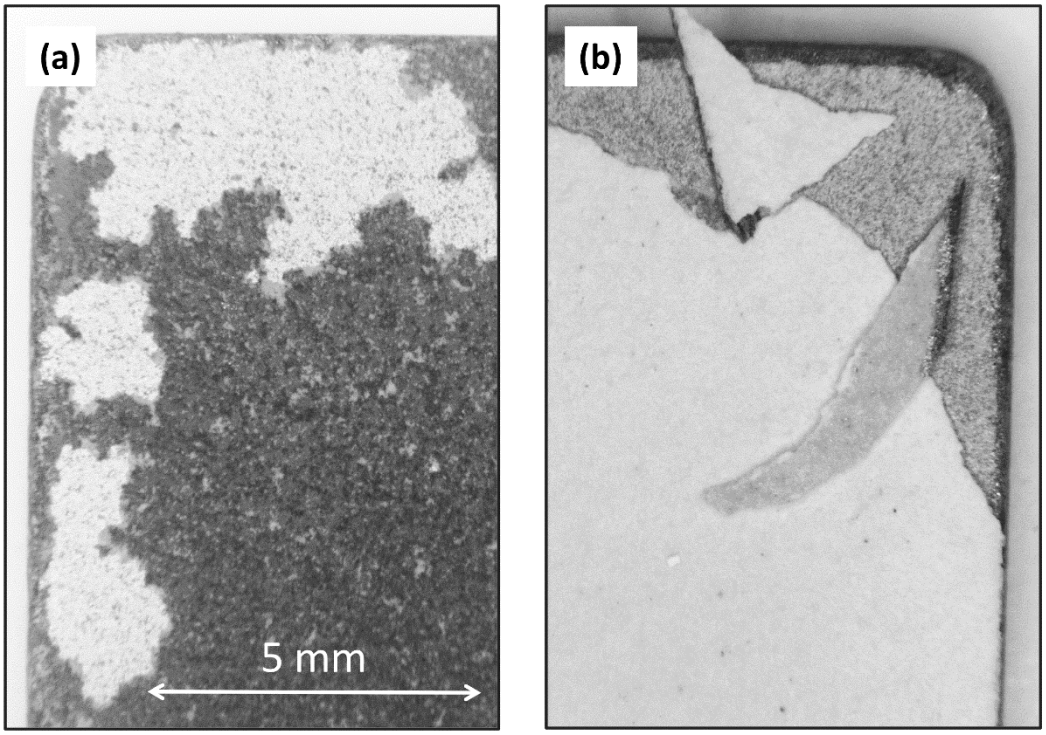

Figure 27.—Interfacial failure for Al_2O_3 scale and YSZ thermal barrier coatings on Kanthal Cr_2AlC. Scale (MIDS) and TBC (DTS) failure initiated here after 400 h at 1150 °C and later completed at 1200 °C. (a) Uncoated side. (b) APS TBC coated side.

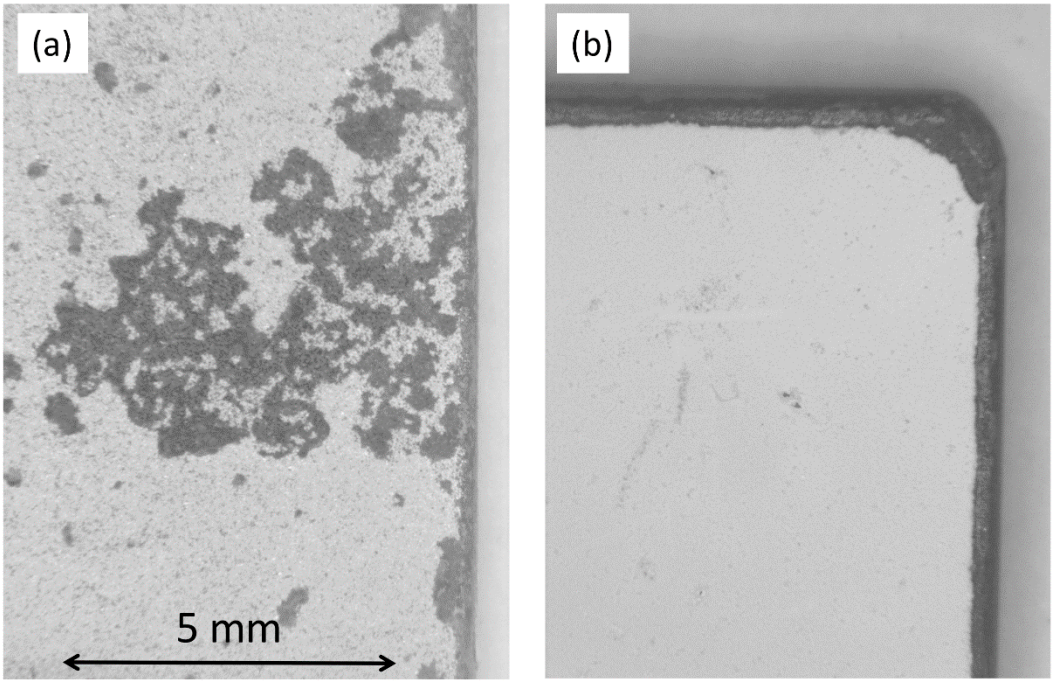

Figure 28.—Interfacial failure for Al_2O_3 scale and intact PS-PVD YSZ thermal barrier coatings on Kanthal Cr_2AlC. Scale (MIDS) failure initiated here after 400 h at 1150 °C. (TBC failure completed at 1200 °C). (a) Uncoated side. (b) PS-PVD TBC coated side.

Compatibility With Superalloys

Cr_2AlC-LSHR, 800 °C/100, 1000 h

If the MAX phases are considered as environmental coatings or bond coats for other load-carrying substrate materials, thermal cycling and interdiffusion need to be considered. MAX phases have often been produced as protective coatings on various Ti, Fe, and Ni-base metals, primarily by magnetron sputtering or high velocity oxy-fuel spraying (HVOF). The deposition, structure, and oxidation of such coatings have been examined in many studies, for example (Refs. 8, 33 to 37). In addition, a few have studied interaction/diffusion with the substrate (Refs. 34 and 36), albeit at lower 700 to 800 °C temperatures. While the specifics of behavior and interactions are too numerous and complex to review here, it is instructive to mention some issues that arise at higher temperatures regarding superalloys.

We have studied the oxidation and interaction of Cr_2AlC-LSHR (low-solvus, high refractory) superalloy disk material as hot-pressed couples (Refs. 25 and 26). It has been shown (at 800 °C, 100 to 1000 h) that a protective Cr_2AlC material reacts with a Ni-base superalloy to form an NiAl + secondary phases interdiffusion zone, leaving an extensive area of Cr_7C_3 depletion zone behind the interface. Both of these features may be considered as a potential detriment from the standpoint of interfacial toughness, though it is pointed out that intermittent thermal cycling did not damage the interface for the extended 1000 h, 800 °C test duration. Also, most of the interdiffusion took place during the 2 h hot press at 1100 °C. It is therefore speculated that diffusional effects may trigger interfacial instabilities at temperatures above 1100 °C.

Here extensive interactions with the Ni-superalloy were found after hot pressing for 2 h at 1100 °C. The interface became "aluminized" by interdiffusion of Ni from the alloy and Al from the Cr_2AlC MAX phase Figure 29. The overall interaction can be characterized as a 10 μm β-NiAl interface intertwined with an "amorphic" Cr_7C_3 40 μm depletion zone in the Cr_2AlC. Furthermore, the NiAl is peppered with Ti(Ta,Nb)C carbides and $W(Mo,Cr)_3B_2$ borides, just as would happen in conventional CVD aluminizing of complex superalloys. The LSHR can also be seen to have an increasing carbide content as the Cr_2AlC interface is approached over an extent of about 50 μm. These diffusion layers did not grow substantially after a 1000 h oxidation anneal at 800 °C. However extensive topologically close packed (TCP) Co, Cr, Mo, W, Ni precipitates did formed in the superalloy near the interface, which may pose an embrittlement concern. Nevertheless, from a mechanical standpoint, it is encouraging that the 0.3 mm Cr_2AlC/1.8 mm LSHR couple withstood 15 cycles to 800 °C, over a 1000 h time period.

Cr_2AlC-N5 1150 °C/20+80 h

In an analogous test, as-received Cr_2AlC Kanthal samples were vacuum diffusion bonded to single crystal Rene′N5 superalloy, ~2 mm thick and 12 mm on a side, each. The hot press conditions were 1100 °C for 2 h with a load ~30 MPa. The hybrid couple was first diffusion annealed in 5% H_2/Ar at 1150 °C for 20 h in order to improve bonding while also producing an initial Al_2O_3 scale with minimal transient components. Bonding occurred over most of the sample surface, but narrow spaces could be discerned at the edges of the couple. Sample test strips ~1.5 mm thick were cut from each edge using a diamond wafering saw. The remaining ~5×10 mm intact sample was then oxidized, intermittently, at 1150 °C for an additional 80 h, after which time the sample delaminated after cooling, eventually.

The weight change response of the bonded couple and separate samples of the same N5 and Cr_2AlC pedigree are shown in Figure 30. All three exhibited a slight gain for the first 20 h in 5% H_2/Ar. A fairly rapid rate ensued for the remainder of the exposure in air, with the hybrid couple higher than the N5 sample and more closely tracking the Cr_2AlC control sample. It is interesting to point out a considerable amount of delayed spallation for Cr_2AlC occurred, as indicated by the multiple reductions in weight at 50 h. These took place over a 24 h period after cooling and are believed to be related to moisture effects as discussed previously.

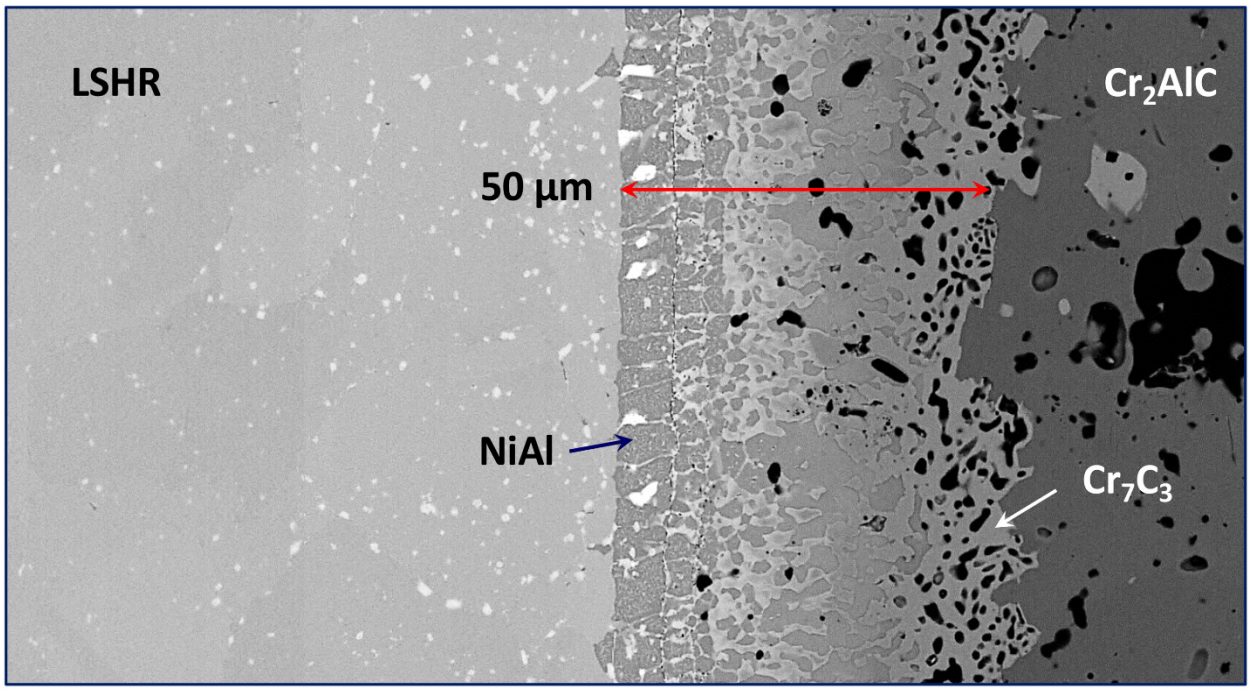

(a)

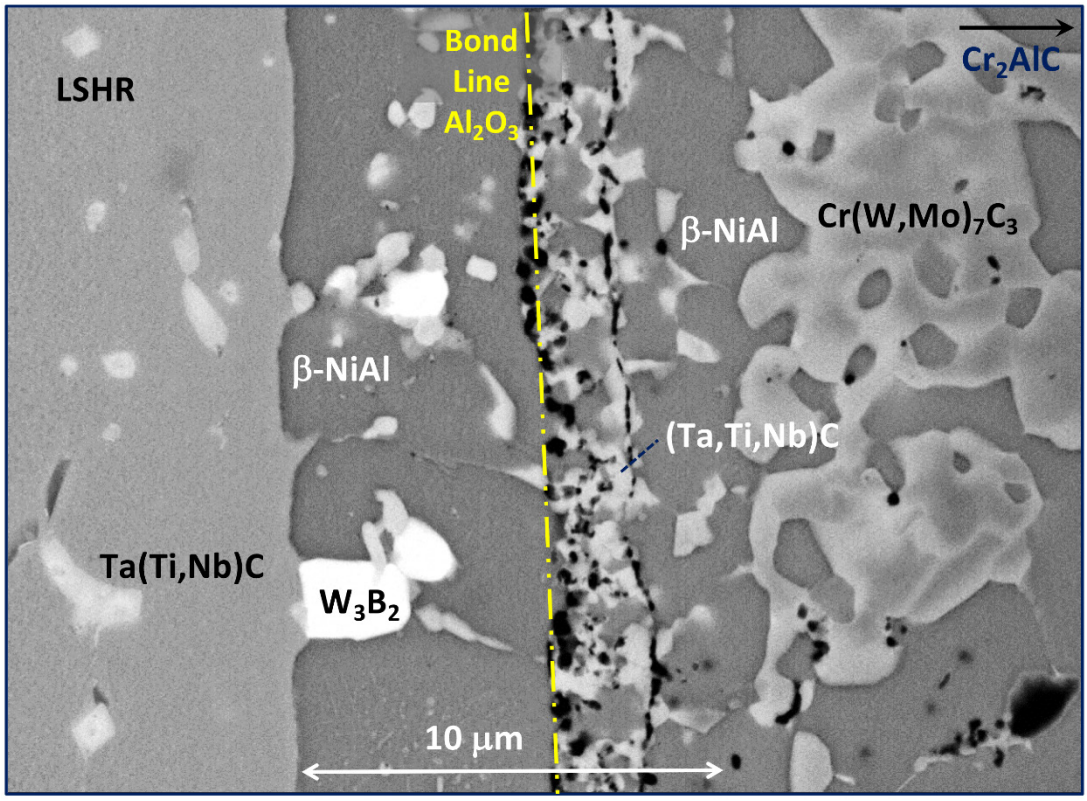

(b)

Figure 29.—Montage of SEM/BSE cross section micrographs: hybrid Cr_2AlC–LSHR superalloy diffusion couple (hot pressed 1100 °C/2 h). (a) 50 µm total interaction zone with NiAl and Cr_7C_3 major phases. (b) 10 µm NiAl interface, with (Ta,Ti,Nb)C and W_3B_2 precipitates (Ref. 26).

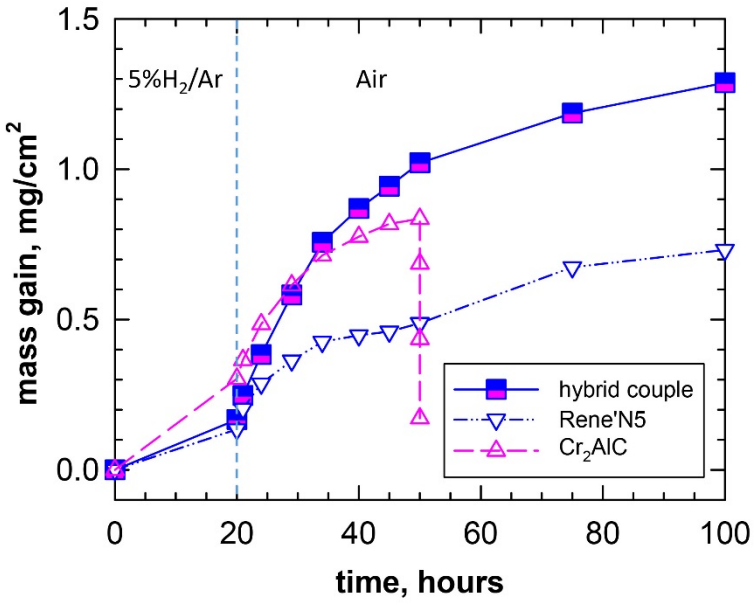

Figure 30.—The 1150 °C oxidation of Rene′N5/ Cr_2AlC hybrid couple (closed symbols), and separate coupons (open symbols).

The edge of the couple was observed by optical microscopy, where the diffusion zone was demarked by changes in the scale morphology, (Fig. 31). Thus the width of the diffusion zone was tracked with time and found to increase considerably, but in a complex fashion, Figure 32. Possible reasons for the complexity are the initial interface growth during hot pressing and difficulty using the scaled appearance of a polished edge to track the multiple layers of the reaction zone. Some agreement was found from measurements obtained from polished cross-sections, Figure 33. Also visible were various features near the interface, still under investigation. In general these appear similar to those formed in similar Cr_2AlC/LSHR interface studies at 800 °C. These exhibited NiAl and Ni_3Al + carbide, aluminized superalloy features, with Cr_7C_3 depletion zones having Al_2O_3 impurities. This band also exhibited partial cracking in some areas, Figure 33(c).

Crack growth and oxidative bond deterioration, coupled with excessive thermal stress, finally separated the couple. XRD analyses identified Cr_2AlC-Cr_7C_3 as the failure locus. This is in contrast to a thin (260 μm) Cr_2AlC-LSHR couple that survived 1000 h intermittent oxidation at 800 °C with no cracks or bond delamination (Ref. 25). Thus some balance of temperature and MAX phase thickness may allow for considerable life at intermediate temperature (e.g., 1100 °C).

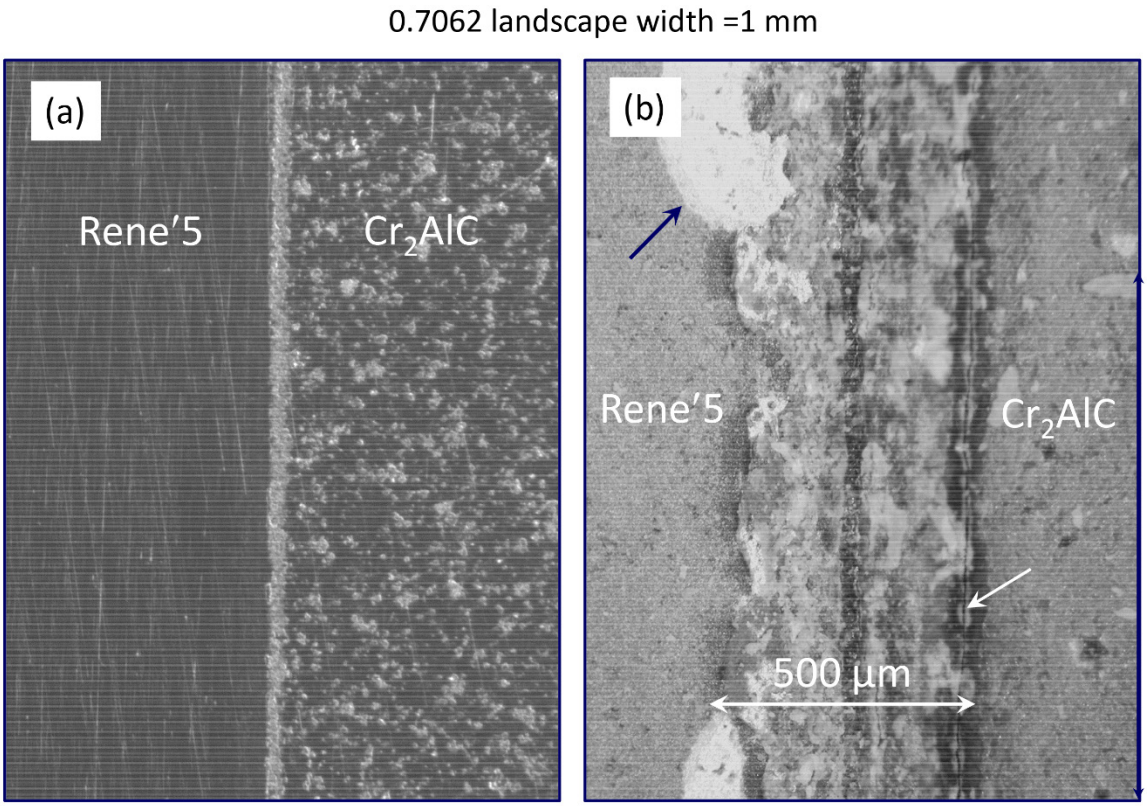

Figure 31.—Polished interface between Rene′N5 and Cr_2AlC hybrid couple (optical). (a) Intact after hot pressing at 1100 °C/2 h. (b) After 1150 °C oxidation for 25 h (6 cycles). Arrows indicate scale spallation, exposed alloy, and crack development, 50x.

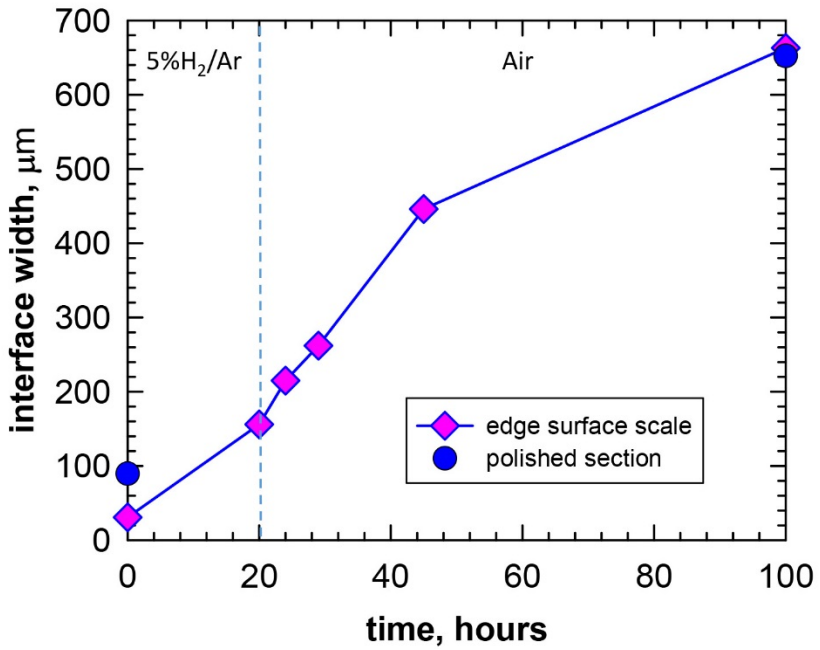

Figure 32.—Rene′N5/Cr_2AlC hybrid couple. Expanding diffusion zone during 1150 °C thermal treatments. Estimated from polished/oxidized edge; endpoints include metallographic cross-section measurements.

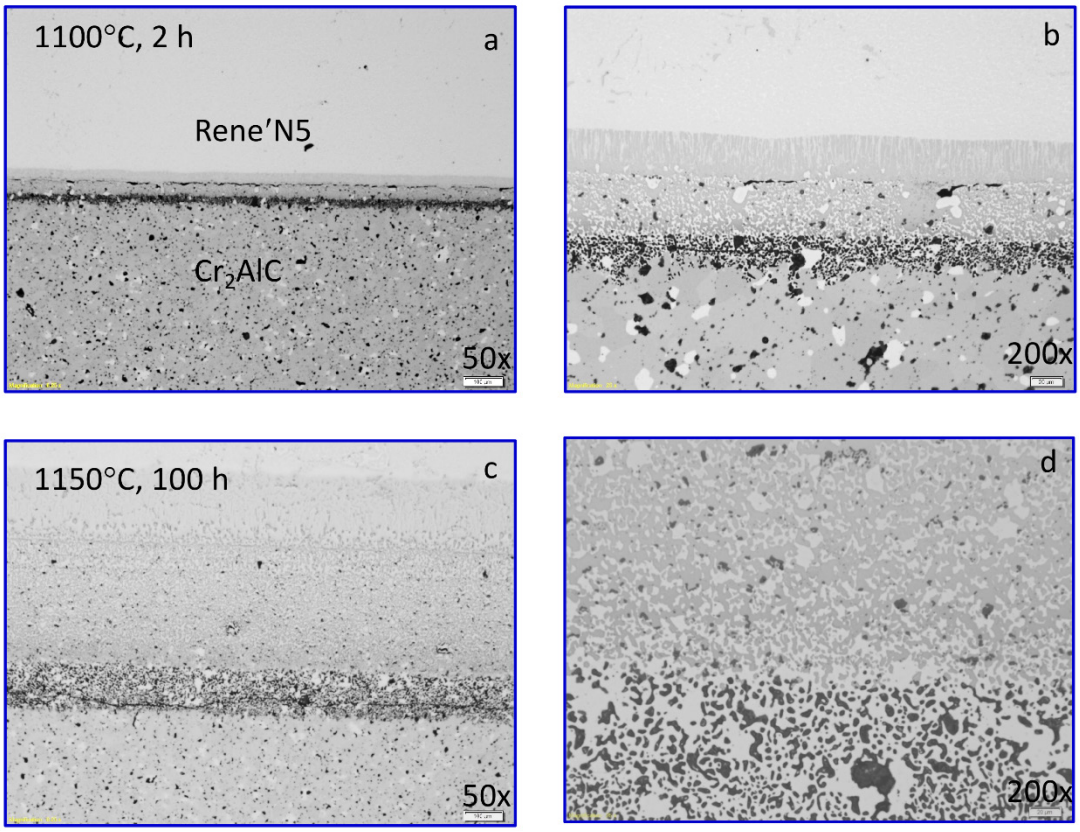

Figure 33.—Polished cross-sections of Rene′N5/Cr2AlC hybrid couple. Growth of diffusion zone after thermal treatments; (a,b) hot pressed at 1100 °C for 2 h; (c,d) after exposures to 1150 °C for 100 h total. 50x scale bar is 100 μm; 200x scale bar is 20 μm.

Discussion

Comments/Solutions/Recommendations

It is remarkable that breakaway oxidation of Ti_2AlC can occur as low as 1100 °C (long term) or in as few as 50 h (re-polished), even though 100 h isothermal tests show slow protective Al_2O_3 kinetics up to 1400 °C. This indicates the sensitivity of these materials to small changes in Al content. Similarly the behavior of Cr_2AlC is very sensitive to interrupted or cyclic exposures above 1100 °C. Massive spallation to an exposed Cr_7C_3 depletion zone eventually affects the regrown scale drastically, such that loss rates eventually become prohibitive. However no damage-initiated breakaway had been observed as with Ti_2AlC, presumably because of the protective effect of a Cr_2O_3 transient scale as compared to non-protective TiO_2.

The preliminary damage studies indicate a potential risk for crushed/deformed Ti-MAX phases. Extreme deformations are most likely accommodated by the classic structures of kinked MAX phase lamellae and delaminations at the basal plane (Refs. 1 and 38). This suggests that separate crystallographic plates are produced at submicron levels with an enormous increase in the exposed surface area. These features may allow rapid attack of all elements in the compound, precluding the healing action of the alumina scale. This is in contrast to a planar, single, continuous surface layer of alumina that forms on a relatively smooth or planar surface.

This damage-initiated attack (at *1200 °C*) can be more insidious and aggressive than Al depletion-induced attack, i.e., by continuous long-term oxidation (3000 h) (Ref. 13) or by atypical cyclic oxidation/re-polishing treatments (50 h) (Ref. 15). The latter are certainly important for they underscore the significance of an adequate level and supply (diffusional flux) of Al to selectively form alumina. However when the surface is disrupted on a submicron level, as with localized crushing damage, the initial Al content is sufficient to form a healing layer of Al_2O_3. That is, the rapid growth of TiO_2 at numerous internal delaminations, per unit of external surface area, kinetically overpowers the slow growth of stable alumina. The widely observed propensity for initial transient TiO_2 formation, occurring on heat-up to ~1000 °C, is an important aspect contributing to this mechanism. Apparently some self-propagating, oxidative growth stress mechanism can promote damage or micro-delamination ahead of the oxidation front, allowing the process to continue or repeat itself. There is, however, a puzzling inconsistency between this detrimental oxidative mechanism for Ti-MAX phases and beneficial oxidative crack-healing in the more-controlled microhardness indent, thermal shock, and fracture tests (Refs. 39 and 40).

It is not guaranteed that any modification would be entirely successful in overcoming the shortcomings above. Breakaway oxidation of Ti_2AlC is correlated with reduced Al contents and a tendency to allow runaway TiO_2 growth with an inability to heal under any transient Ti scales. Foremost, rough machined or damaged surfaces should be avoided when possible. However some mechanical damage triggers may not be avoidable and need compositional means of protection. In this regard, some alloying with Cr_2AlC may be helpful, since any Cr_2O_3 transient scales would have a greater likelihood of curtailment than fast growing TiO_2. Small excess Si additions may also serve to curtail transient TiO_2, but possibly at some penalty to mechanical properties.

Conversely, the addition of Ti_2AlC to Cr_2AlC may improve scale adhesion. It would provide a somewhat better expansion match to the scale and may also improve the chemical bond strength of the scale to the substrate. Reactive element dopants (Y, Zr, Hf) are a primary choice for scale adhesion because of their known effectiveness in gettering sulfur, (if that is critical here), strengthening the bond, and slowing scale growth on metallic substrates. Such an approach is already in progress in the current studies of Sloof et al.

The Cr_7C_3 impurity phase in Cr_2AlC has been associated with degraded oxidation, corrosion, and increased scale volatility. It is not especially evident how to reduce this phase since it depends heavily on processing steps that may be specific to each laboratory. As a generalization, it might be recommended to increase the Al content of the various starting mixes and drive away from Cr-rich secondary phases. Eliminating the Cr_7C_3 phase would also eliminate Cr_2O_3-based scale volatility for Cr_2AlC in oxygen as CrO_3 or water vapor as $Cr_2O_2(OH)_2$. Similarly, additions of Cr_2AlC to Ti_2AlC would limit TiO_2 volatility by reducing the amount of initial TiO_2 transient as discussed before.

Both Cr_2AlC additions to Ti_2AlC and Ti_2AlC additions to Cr_2AlC can be envisioned to improve TBC oxidative life on each substrate. The former by minimizing TiO_2 transients and breakaway, the latter by improved CTE match and TGO bonding. Reactive element doping may be useful in the latter regard.

Interdiffusion, reactions, and mechanical instability as coatings on other metal or CMC substrates probably cannot be reduced by any meaningful amount. Therefore practical temperature limits would need to be defined for metal (superalloys) and ceramic (SiC) substrates. Layer thickness must be such that it survives thermal cycling and retains enough MAX phase for property benefits. It would have to be co-optimized for balanced properties: too thin leaving little MAX phase after interdiffusion, too thick causing delamination from high interfacial shear stresses. Should the MAX phases be mechanically unstable with SiC or CMCs at any thickness, they may be more useful as an in-situ self-healing oxide precursor, hopefully preventing oxidation of fibers after first matrix cracking or rapid moisture attack of susceptible BN interfacial fiber coatings.

Summary and Conclusions

Alumina-forming MAX phases possess many desirable features for environmental durability in high temperature oxidizing conditions approaching 1400 °C. While most exposures can be endured with little evidence of degradation, others may initiate near-catastrophic behavior. Accelerated oxidation of Ti_2AlC has been shown to occur for Al-depleted, damaged (EDM, punch, or diamond scribe), or 180 grit roughened surfaces at temperatures ≤1200 °C. These all stem from a propensity to produce fast growing TiO_2 scales without effective Al_2O_3 healing.

Cr_2AlC is less sensitive to this breakaway oxidation, but may suffer from Cr_2O_3 formed over Cr_7C_3 impurity phases. These regions can produce volatile CrO_3 losses at 1200 °C or above. Also, scale spallation eventually occurs after cooling from oxidation at 1150 °C or above, exposing the ubiquitous Cr_7C_3 depletion zone phase. Delayed spallation is significant and suggests a moisture-induced phenomenon similar to scales formed on non-adherent metallic systems. Attempts to improve adhesion by hydrogen annealing were unsuccessful. Re-oxidation of this surface does not produce Al_2O_3, but initiates a less-protective Cr-rich scale with ever-increasing rates of spallation. This cyclic oxidation deficit is in stark contrast to the excellent spallation resistance noted for Ti_2AlC and Ti_3AlC_2 compounds.

Lastly, Cr_2AlC is mechanically compatible with superalloys at 800 °C (1000 h), but not for very long at 1100 °C or above (100 h). Diffusion couples exhibited significant β-NiAl + Cr_7C_3 diffusion zones at 1100 and 1150 °C. Along with the increase in thermal stress at higher temperatures, this interface instability and weakness may contribute to delamination failure on cooling.

References

1. M.W. Barsoum, T. El-raghy, The MAX Phases: Unique New Carbide and Nitride Materials, Am. Sci. 89 (2001) 334–343.
2. D.J. Tallman, B. Anasori, M.W. Barsoum, A Critical Review of the Oxidation of Ti_2AlC, Ti_3AlC_2 and Cr_2AlC in Air, Mater. Res. Lett. 1 (2013) 115–125. doi:10.1080/21663831.2013.806364.
3. X.H. Wang, Y.C. Zhou, High-Temperature Oxidation Behavior of Ti_2AlC in Air, Oxid. Met. 59 (2003) 303–320.
4. X.H. Wang, Y.C. Zhou, Oxidation behavior of Ti_3AlC_2 at 1000–1400 °C in air, Corros. Sci. 45 (2003) 891–907. doi:10.1016/S0010-938X(02)00177-4.
5. Z. Lin, M. Zhuo, Y. Zhou, M. Li, J. Wang, Microstructures and Adhesion of the Oxide Scale Formed on Titanium Aluminum Carbide Substrates, J. Am. Ceram. Soc. 89 (2006) 2964–2966. doi:10.1111/j.1551-2916.2006.01141.x.
6. X.K. Qian, X.D. He, Y.B. Li, Y. Sun, H. Li, D.L. Xu, Cyclic oxidation of Ti_3AlC_2 at 1000–1300 °C in air, Corros. Sci. 53 (2011) 290–295. doi:10.1016/j.corsci.2010.09.033.
7. G.M. Song, V. Schnabel, C. Kwakernaak, S. van der Zwaag, J.M. Schneider, W.G. Sloof, High temperature oxidation behaviour of Ti_2AlC ceramic at 1200 °C, Mater. High Temp. 29 (2012) 205–209. doi:10.3184/096034012X13348496462140.
8. J. Frodelius, J. Lu, J. Jensen, D. Paul, L. Hultman, P. Eklund, Phase stability and initial low-temperature oxidation mechanism of Ti_2AlC thin films, J. Eur. Ceram. Soc. (2013).
9. J.L. Smialek, Kinetic Aspects of Ti_2AlC MAX Phase Oxidation, Oxid. Met. 83 (2015) 351–366. doi:10.1007/s11085-015-9526-7.
10. J.L. Smialek, Environmental resistance of a Ti_2AlC-type MAX phase in a high pressure burner rig, J. Eur. Ceram. Soc. (2016). doi:10.1016/j.jeurceramsoc.2016.07.038.
11. X.H. Wang, F.Z. Li, J.X. Chen, Y.C. Zhou, Insights into high temperature oxidation of Al_2O_3-forming Ti_3AlC_2, Corros. Sci. 58 (2012) 95–103. doi:10.1016/j.corsci.2012.01.011.
12. J.L. Smialek, Oxygen diffusivity in alumina scales grown on Al-MAX phases, Corros. Sci. 91 (2015) 281–286. doi:10.1016/j.corsci.2014.11.030.

13. X. Li, L. Zheng, Y. Qian, J. Xu, M. Li, Breakaway oxidation of Ti_3AlC_2 during long-term exposure in air at 1100 °C, Corros. Sci. 104 (2016) 112–122. doi:10.1016/j.corsci.2015.12.001.
14. J.L. Smialek, B.J. Harder, A. Garg, Oxidative durability of TBCs on Ti_2AlC MAX phase substrates, Surf. Coatings Technol. 285 (2016) 77–86. doi:10.1016/j.surfcoat.2015.11.018.
15. X. Li, Y. Qian, L. Zheng, J. Xu, M. Li, Determination of the critical content of Al for selective oxidation of Ti_3AIC_2 at 1100 °C, J. Eur. Ceram. Soc. 36 (2016) 3311–3318.
16. J. Xu, Z. Gao, Y. Qian, M. Li, Ultra-High-Temperature Oxidation and Thermal Stability of Ti_2AlC in Air at 1600–1800 °C, Oxid. Met. 86 (2016) 327–338. doi:10.1007/s11085-016-9639-7.
17. P. Saltykov, O. Fabrichnaya, J. Golczewski, F. Aldinger, Thermodynamic modeling of oxidation of Al-Cr-Ni alloys, J. Alloys Compd. 381 (2004) 99–113. doi:10.1016/j.jallcom.2004.02.053.
18. N.S. Jacobson, M.P. Brady, G.M. Mehrotra, Thermodynamics of Selected Ti-Al and Ti-Al-Cr Alloys, Oxid. Met. 52 (1999) 537–556. doi:10.1023/a:1018820401533.
19. J.L. Smialek, Oxidation behaviour of $TiAl_3$ coatings and alloys, Corros. Sci. 35 (1993) 1199–1208. doi:10.1016/0010-938X(93)90340-M.
20. J. Smialek, A. Garg, R. Rogers, R. Noebe, Oxide Scales Formed on NiTi and NiPtTi Shape Memory Alloys, Metall. Mater. Trans. A. 43 (2012) 2325–2341. doi:10.1007/s11661-011-1036-x.
21. S. Basu, N. Obando, A. Gowdy, I. Karaman, M. Radovic, Long-Term Oxidation of Ti_2AlC in Air and Water Vapor at 1000–1300 °C Temperature Range, J. Electrochem. Soc. 159 (2012) C90. doi:10.1149/2.052202jes.
22. Q.N. Nguyen, D.L. Myers, N.S. Jacobson, E.J. Opila, Experimental and Theoretical Study of Thermodynamics of the Reaction of Titania and Water at High Temperatures; NASA/TM—2014-218372, Cleveland, OH, 2014.
23. J.L. Smialek, Diffusivity in Alumina Scales Grown on Al-MAX Phases, NASA/TM—2014-218344. (2014) 1–10. http://sti.nasa.gov.
24. D.B. Lee, S.W. Park, Oxidation of Cr_2AlC Between 900 and 1200 °C in Air, Oxid. Met. 68 (2007) 211–222. doi:10.1007/s11085-007-9071-0.
25. J.L. Smialek, A. Garg, Interfacial reactions of a MAX phase / superalloy hybrid, Surf. Interface Anal. 47 (2015) 844–853. doi:10.1002/sia.5784.
26. J.L. Smialek, A. Garg, Microstructure and Oxidation of a MAX Phase / Superalloy Hybrid Interface, NASA TM 2014-216679. (2014) 1–19.
27. D.B. Lee, T.D. Nguyen, J.H. Han, S.W. Park, Oxidation of Cr_2AlC at 1300 °C in air, Corros. Sci. 49 (2007) 3926–3934. doi:10.1016/j.corsci.2007.03.044.
28. Z.J. Lin, M.S. Li, J.Y. Wang, Y.C. Zhou, High-temperature oxidation and hot corrosion of Cr_2AlC, Acta Mater. 55 (2007) 6182–6191. doi:10.1016/j.actamat.2007.07.024.
29. J.K. Tien, F.S. Pettit, Mechanism of oxide adherence on Fe-25Cr-4Al (Y or Sc) alloys, Metall. Trans. 3 (1972) 1587–1599. doi:10.1007/BF02643050.
30. J.L. Smialek, Enigmatic Moisture Effects on Al_2O_3 Scale and TBC Adhesion, Mater. Sci. Forum. 595–598 (2008) 191–198. doi:10.4028/www.scientific.net/MSF.595-598.191.
31. J. Smialek, Maintaining adhesion of protective Al_2O_3 scales, JOM. 52 (2000) 22–25. doi:10.1007/s11837-000-0110-4.
32. D.B. Lee, T.D. Nguyen, Cyclic oxidation of Cr_2AlC between 1000 and 1300 C in air, J. Alloys Compd. 464 (2008) 434–439. doi:10.1016/j.jallcom.2007.10.018.
33. C. Walter, D.P. Sigumonrong, T. El-Raghy, J.M. Schneider, Towards large area deposition of Cr_2AlC on steel, Thin Solid Films. 515 (2006) 389–393. doi:10.1016/j.tsf.2005.12.219.
34. Q.M. Wang, A. Flores Renteria, O. Schroeter, R. Mykhaylonka, C. Leyens, W. Garkas, M. to Baben, Fabrication and oxidation behavior of Cr_2AlC coating on Ti6242 alloy, Surf. Coatings Technol. 204 (2010) 2343–2352. doi:10.1016/j.surfcoat.2010.01.002.
35. D.E. Hajas, M. to Baben, B. Hallstedt, R. Iskandar, J. Mayer, J.M. Schneider, Oxidation of Cr_2AlC coatings in the temperature range of 1230 to 1410 °C, Surf. Coatings Technol. 206 (2011) 591–598. doi:10.1016/j.surfcoat.2011.03.086.

36. J.J. Li, M.S. Li, H.M. Xiang, X.P. Lu, Y.C. Zhou, Short-term oxidation resistance and degradation of Cr_2AlC coating on M38G superalloy at 900–1100 °C, Corros. Sci. 53 (2011) 3813–3820. doi:10.1016/j.corsci.2011.07.032.
37. M. Sonestedt, J. Frodelius, M. Sundberg, L. Hultman, K. Stiller, Oxidation of Ti_2AlC bulk and spray deposited coatings, Corros. Sci. 52 (2010) 3955–3961. doi:10.1016/j.corsci.2010.08.004.
38. W. Yu, S. Li, W.G. Sloof, Microstructure and mechanical properties of a $Cr_2AlC(Si)C$ solid solution, Mater. Sci. Eng. A. 527 (2010) 5997–6001. doi:10.1016/j.msea.2010.05.093.
39. G.M. Song, Y.T. Pei, W.G. Sloof, S.B. Li, J. Th, M. De Hosson, Oxidation-induced crack healing in Ti_3AlC_2 ceramics, 58 (2008) 13–16. doi:10.1016/j.scriptamat.2007.09.006.
40. S. Li, G. Song, K. Kwakernaak, S. van der Zwaag, W.G. Sloof, Multiple crack healing of a Ti_2AlC ceramic, J. Eur. Ceram. Soc. 32 (2012) 1813–1820. doi:10.1016/j.jeurceramsoc.2012.01.017.